Hybrid ensemble artificial intelligence algorithms for predicting peak shear strength of clayey soil-geomembrane interfaces and experimental validation

Zhiming Chao[1,2,3,4#], Danda Shi[1#], Gary Fowmes[4]*, Xu Xu[5], Wenhan Yue[5], Peng Cui[3], Tianxiang Hu[1], Chuanxin Yang[1]

[1] Shanghai Maritime University, Shanghai, China, 200135

[2] Failure Mechanics and Engineering Disaster Prevention, Key Laboratory of Sichuan Province, Sichuan University, Chengdu, China, 610065

[3] School of Civil Engineering, Nanjing Forestry University, Nanjing, China, 210037

[4] School of Engineering, University of Warwick, Coventry, UK, CV4 7AL

[5]Anhui Provincial Port and Shipping Group Co.,LTD,

[*] Corresponding author, E-mail: zmchao@shmtu.edu.cn

[#] The authors contribute equally to this paper

Abstract

The peak shear strength of clayey soil-geomembrane interfaces is a vital parameter for the design of relevant engineering infrastructure. However, due to the large number of influence factors and the complex action mechanism, accurate prediction of the peak shear strength for clayey soil-geomembrane interfaces is always a challenge. In this paper, a novel machine learning model was established by combining Mind Evolutionary Algorithm (MEA) and the ensemble algorithm of Adaptive Boosting Algorithm (ADA)-Back Propagation Artificial Neural Network (BPANN) to predict the peak shear strength of clayey soil-geomembrane interfaces based on the results of 623 laboratory interface direct shear experiments. By comparing with the conventional machine learning algorithms, including Particle Swarm Optimisation Algorithm (PSO) and Genetic Algorithm (GA) tuned ADA-BPANN, MEA tuned Support Vector Machine (SVM) and Random Forest (RF), the superior performance of MEA tuned ADA-BPANN has been validated, with higher predicting precision, shorter training time, and the avoidance of local optimum and overfitting. By adopting the proposed novel model, sensitivity analysis was carried out, which indicates that normal pressure has the largest influence on the peak shear strength, followed by geomembrane roughness. Furthermore, an analytical equation was proposed to assess the peak shear strength that allows the usage of machine learning skills for the practitioners with limited machine learning knowledge. The present research highlights the potential of the MEA tuned ADA-BPANN model as a useful tool to assist in preciously estimating the peak shear strength of clayey soil-geomembrane interfaces, which can provide benefits for the design of relevant engineering applications.

Keywords: Clayey Soil; Geomembrane; Interfaces; Peak shear strength

1. Introduction

Geomembranes are widely applied in hydraulic engineering, civil engineering and other engineering fields(Biabani and Indraratna, 2015; Cazzuffi and Gioffrè, 2020; Koerner and Koerner, 2006; Yu and Rowe, 2018), and in order for them to operate effectively they must interact with surrounding materials, such as soil, etc. through interfaces (Abdelaal et al., 2019; Eldesouky and Brachman, 2018; Rowe et al., 2009; Rowe and Shoaib, 2017). For the engineering applications installed with geomembranes, soil-geomembrane interfaces are often their weakest component, and the peak shear strength of soil-geomembrane interfaces decides the stability of the engineering facilities (Chao and Fowmes, 2021; Chen et al., 2021; Eldesouky and Brachman, 2020). For example, the peak shear strength for clayey soil-geomembrane interfaces in landfill cover systems determines the stability of landfills (Mirzababaei et al., 2017). Thus, a correct assessment of the peak shear strength for soil-geomembrane interfaces is vital for the reasonable design and safe operation of relevant engineering applications.

Conducting direct shear tests is the primary method to determine the peak shear strength of soil-geomembrane interfaces (Abdelaal and Solanki, 2022; Punetha et al., 2017). Many scholars have measured the peak shear strength of soil-geomembrane interfaces based on direct shear experiments (Ghazizadeh and Bareither, 2018; Lopes et al., 2014; Makkar et al., 2017; Mehrjardi and Motarjemi, 2018; Sharma et al., 2007; Suzuki et al., 2017). The studies show that the properties of soil such as mean particle size, density, etc., and the characteristics of geomembrane such as roughness, density, etc. as well as normal stress have relatively large impacts on the peak shear strength of soil-geomembrane interfaces(Biabani and Indraratna, 2015; Chao and Fowmes, 2022; Rowe and Jabin, 2021; Vangla and Gali, 2016). However, geosynthetics interface testing is expensive and time consuming, and the exact materials to be deployed on site are often chosen well after the design stage, thus, there is a clear need to develop an effective method to predict the peak shear strength of soil-geomembrane according to the typical charaterics of soil and geomembrane. Hence, based on the results of direct shear tests, a number of researchers have attempted to develop prediction models to evaluate the peak shear strength of soil-geomembrane interfaces by taking the aforementioned important parameters of soil and geomembrane as the input parameters (Ghazavi and Bavandpouri, 2022; Pant and Ramana, 2022; Raja and Shukla, 2021). However, due to the complicated action mechanism between soil and geomembrane as well as the large number of influence factors, most of the forecasting models established by adopting traditional function fitting or analytical methods cannot comprehensively reflect the impacts of multiple factors on the peak shear strength along soil-geomembrane interfaces (Chao et al., 2021). For example, Liu et al. (2009) proposed an analytical model to forecast the interface shear resistance between soil and geogrid, which considers the influence of three variables including the opening area of geogrid ribs and shear strength of soil, etc. on the interface shear resistance. He et al. (2021) established an empirical model to estimate the peak shear strength of clayey soil-concrete interfaces, with taking two variables about the material properties of the interface as the input parameters. He et al. (2019) used an analytical model that takes two experimental variables into account to foretell the peak shear strength of soil-geogrid interfaces. Based on the above analysis, the peak shear strength predictive models that are established by using the traditional function fitting or analytical methods only can consider the influence of a small number of variables, which cannot establish the complex relationship between a large number of variables.

Artificial intelligence techniques can model the complex relationship between multiparameters, with a high precision and efficiency. Therefore, in recent years, an increasing number of researchers have utilised machine learning techniques to solve various geotechnical issues (Al-Mudhafar, 2017; Chao et al., 2022; Debnath and Dey, 2017; Erofeev et al., 2019; Kumar and Basudhar, 2018; Sudakov et al., 2019). The effectiveness of machine learning algorithms in modelling complex geotechnical issues between many variables have been extensively validated (Abad et al., 2022; Çalışkan et al., 2022; Choubineh et al., 2017; Erofeev et al., 2019; Ghorbani et al., 2017; Sudakov et al., 2019). For example, Asteris et al. (2021) firstly used the machine learning algorithms of AdaBoost and Random Forestry (RF) to predict the compressive strength of cement-based mortars, which has better assessing accuracy than that of traditional methods. Sathyan et al. (2020) modelled the shear flow behaviour of cement paste by combining machine learning techniques (XGBoostas) and physical experiments, and the research indicates that the model developed by using XGBoost is a promising tool for solving highly complex and heterogeneous geotechnical engineering problems. However, due to the lack of modelling data, reports containing the application of machine learning methods in predicting the peak shear strength of interfaces between soil and geosynthetics are rare. In the limited research, the authors adopted machine learning techniques to establish models for assessing the peak shear strength of clayey soil-geocomposite drainage layer interfaces (Chao et al., 2021). However, the existing research about the modelling of peak shear strength for soil-geosynthetics interfaces has two main deficiencies. Firstly, the studies do not involve machine learning modelling of the peak shear strength along soil-geomembrane interfaces. Secondly, the existing investigation mainly utilised some common and straightforward machine learning algorithms, and the applicability of more advanced and sophisticated machine learning algorithms, such as the ensemble algorithms of Adaptive Boosting Algorithm-Back-propagation Artificial

Neural Network (ADA-BPANN) and Random Forest (RF) in evaluating the peak shear strength of interfaces has not been explored.

In general, the machine learning models without combining optimization algorithms are inefficient, with slow convergence speed, overtraining, or prone to converging to local optima, and often pose a convergence problem (Ebrahimi et al., 2016; Raja and Shukla, 2020; Saghatforoush et al., 2016; Yao et al., 2010). More importantly, there is subjectivity in the artificially determining of initial model parameters, which causes low predictive accuracy (Hasanipanah et al., 2018). Hence, the optimised algorithms, such as, Genetic Algorithm (GA) and Particle Swarm Optimisation Algorithm (PSO) were applied by some researchers to optimise the initial parameters of machine learning models for evaluating the properties of geotechnical materials, and the increase in both of predictive accuracy and convergence speed of the constructed machine learning models after combining optimisation algorithms has been demonstrated (Ahmadi and Chen, 2019; Al Khalifah et al., 2020). However, GA and PSO still have some inherent drawbacks. For example, their computational efficiency is low with long operational time, and they cannot guarantee the gained result is globally optimum, causing detrimental impacts on their optimisation effects (Liu et al., 2015; Wang and Shen, 2018). To solve the shortcomings, many works have been carried out by scholars, among of which is, Sun et al. (2000) proposed Mind Evolutionary Algorithm (MEA) to overcome the aforementioned defects of GA and PSO and improve the optimisation effects (Jie et al., 2004; Xie et al., 2000). The better performance of MEA than that of GA and PSO on increasing the estimating accuracy of machine learning models has been proved by researchers in engineering field (Liu et al., 2015; Wang et al., 2018; Xu et al., 2018). For example, Zhang et al. (2022) integrated BPANN and MEA to conduct back analysis of the surrounding rock parameters, which presented superior predictive performance than that of traditional machine learning algorithms. Wang et al. (2019) combined the ecological restoration experiment for soil contamination and MEA tuned ANN to estimate the heavy metal content of soil, and the research indicates that the MEA tuned algorithm has satisfying precision. Wang et al. (2018) compared the prediction performance and generalization capabilities of MEA-BPANN with the GA-BPANN model in estimating the height of ocean waves. The study results demonstrate that the MEA-BPANN model performs better than the GA-BPANN model and BPANN model, with faster running time and higher prediction accuracy. However, to the best knowledge of the authors, currently, the application of MEA in improving the performance of machine learning models for predicting the peak shear strength of soil-geosynthetics interfaces has not been reported, let alone assessing the peak shear strength along soil-geomembrane interfaces.

In this paper, based on the database constructed upon the 623 large direct shear experiments on clayey soil-geomembrane interfaces, a novel machine learning model for forecasting the peak shear strength of clayey soil-geomembrane interfaces was proposed by combining MEA and ADABPANN. To justify the superior performance of the novel model compared to the conventional machine learning algorithms, the GA and PSO tuned BPANN, MEA tuned SVM and RF models were constructed and compared with the MEA tuned ADABPANN. Furthermore, the sensitivity analysis was conducted and an analytical equation was built to facilitate the peak shear strength evaluation for geotechnical engineers with limited machine learning learnings. The novel machine learning model established in this research aims to provide more accurate, efficient and reliable predictions of peak shear strength for clayey soil-geomembrane interfaces, which is also the key to improve the design quality of relevant buildings.

2. Machine learning algorithms

There are four types of machine learning algorithms including BPANN, SVM, ADA-BPANN and RF, that were adopted in this paper. A brief introduction of the used machine learning algorithms was conducted in the following.

2.1 BPANN

BPANN is a multi-layer feed-forward neural network based on error back propagation algorithm, the typical structure of BPANN model. The BPANN model utilized in this study is comprised of three layers: input layer, hidden layer, and output layer. The input and output layers of the model is composed of five joints and one joint, respectively. The number of hidden-layer joints in the model was determined by a loop program. In this program, firstly, BPANN models with a hidden joint size ranging from 1 to 1000 were established by the training dataset. Then, the predictive accuracies of models with different hidden-layer sizes were evaluated using the testing dataset according to the assessment indicator of Root-Mean-Square Error (RMSE), as expressed in Equation (1). Subsequently, the hidden layer joint size of the model with the least RMSE was selected as the optimal hidden layer joint size. In this case, the optimal hidden layer joint size was nine. The activation function and network training algorithm in the proposed BPANN model are Logarithmic Sigmoid Function and Levenberg-Marquardt Backpropagation Algorithm, respectively, with the initial weights and thresholds of joints in the BPANN model being optimized.

$$RMSE = \sqrt{\sum_{i=1}^{n} \frac{(y_i - f_i)^2}{n}} \quad (1)$$

Where, n is the number of sample data, y_i is measured value, f_i is predictive value.

2.2 SVM

SVM is a binary predictive model, which is able to divide and predict sample data to achieve structural risk minimization according to maximum margin principles. SVM can achieve high forecasting accuracy based on few data sample. In this case, the radial basis function was selected as the kernel function of the SVM model, with penalty parameter c and g of the kernel function being optimized.

2.3 ADA-BPANN

ADA-BPANN is one type of robust ensemble algorithms that consists of many “weak” base learners (BPANN models) to form a “strong” predictive model with a better forecasting performance (Shen et al., 2020). The training process of ADA-BPANN, as follows: (1) Establish single BPANN model (base leaner) based on original training data (2) allocate more weight on the training data with wrong predictive value depending on the predictive performance of the base learners (3) establish new base learners according to the adjusted training data (4) repeat Step (2) and Step (3) until the predetermined number of base learners are established (5) calculate predictive results of the established base learners adopting weighed average method to obtain the final predictive results. The BPANN models in ADA-BPANN has the same structure and parameter specification with 5 input layer joints, 9 hidden layer joints and 1 output layer joint, taking Logarithmic Sigmoid Function as the activation function and Levenberg-Marquardt Backpropagation Algorithm as the network training algorithm, with the number of BPANN models in the

ADA-BPANN model and the initial weights/thresholds of joints in the BPANN models being optimised, respectively.

2.4 RF

RF is another ensemble algorithm that is constituted of a group of Decision Tree (DT) models based on Bootstrap aggregating technique (Liaw and Wiener, 2002). The training process of RF as follows: (1) Generate a number of different training datasets and testing datasets using Bootstrap method (2) establish DT models according to the training datasets, respectively (3) input corresponding testing datasets into the constructed DT models to obtain the predictive results, respectively (4) calculate the average value of predictive results from the established DT models as the final predictive values of RF model. The main advantages of adopting RF include: (i) simple operation method (ii) low computational cost (iii) high predictive accuracy and generalised ability (Kohestani et al., 2015). Two parameters were optimised in the RF model: the number of DT models and the minimum number of samples in the leaf node of DT models, respectively.

3. Hyperparameters optimization

All machine learning algorithms have several crucial hyper-parameters that can influence their predictive performance significantly. Hence, it is necessary to optimise the hyper-parameters of machine learning algorithms before training of them. In this research, MEA was adopted to optimise the hyperparameters of the constructed machine learning models, with RMSE as the fitness function. MEA is a new heuristically evolutionary intelligence algorithm, which was proposed by Sun et al.(2000). MEA can overcome the inherent defects of traditional evolutionary intelligence algorithms of GA and PSO, such as low computational efficiency, long operational time, obtaining local optimum (Jie et al., 2004;

Xie et al., 2000), which has been proved by researchers in engineering fields (Liu et al., 2015; Wang and Shen, 2018; Wang et al., 2018; Xu et al., 2018; Zhao et al., 2016). MEA has several main advantages: (i) The computational efficiency is high due to the parallel computation of similartaxis and dissimilation operations. (ii) The evolutionary information that MEA can retain is more than one generation, which provides beneficial guidance on the operational directions of similartaxis and dissimilation operations. (iii) The similartaxis and dissimilation operations in MEA can avoid the damage of original information for individuals. Similartaxis refers to that firstly, the fitness value of individuals is evaluated, and based on the evaluated fitness value, the individuals are divided as superior individuals and temporary individuals. Then, new individuals are generated around the superior individuals and temporary individuals. After that, the fitness value of new individuals is evaluated, and based on the fitness value, all the individuals are divided as superior individuals and temporary individuals again.

The specific operation of adopting MEA to optimise machine learning models as follows: (1) Randomly generate individuals that are composed of different hyperparameter values in the solution space (2) score the individuals based on fitness values (RMSE) obtained by calling the corresponding machine learning model, and divide the individuals with low RMSE value as superior individuals and other individuals with high RMSE value as temporary individuals (3) assign the superior individuals and temporary individuals as centres, respectively, then generate new individuals around each centre individual to obtain superior subgroups and temporary subgroups, respectively (4) perform similartaxis operations in each subgroup until the subgroup is mature (the RMSE value of the subgroup keeps unchangeable during continuous 6 times iteration), and take the RMSE value of the optimal individual (centre individual) in each subgroup as the RMSE value of corresponding subgroups (5) when the subgroups are all mature, post the RMSE value of each subgroup on the global bulletin board, and conduct dissimilation operations between the superior subgroups and temporary subgroups, including replacing or abandoning subgroups, releasing individuals in abandoned subgroups, and supplying new subgroups (6) carry out similartaxis operations in the new supplying subgroups, and repeat Step (4) to Step (5) until the RMSE value of new supplying subgroups is lower than those of superior subgroups, respectively (6) take the centre individual in the superior subgroup with the lowest RMSE as the global superior individual, and assign the hyperparameter values of the global superior individual as the initial hyperparameter values of the established machine learning model (7) train the built machine learning model, and conduct prediction, the detailed optimising process as shown in Figure 1.

In this case, the population size was set as 300, and the number of superior subgroups and temporary subgroups was the same, with being set as 3. The size of subgroup is 30, and the maximum iteration number is 20. Additionally, the fitness function value (RMSE) of individuals in MEA was obtained using *k*-fold cross-validation method (*k*-CV) on the corresponding machine learning model during the process of hyperparameter optimisation. *k*-CV is an extensively adopted method to validate the performance of machine learning models, which refers to that the original data are divided into equal *k* groups. The training of machine learning models is based on *k*-1 groups, while the validation is conducted on the remaining 1 group. The training and validating process is repeated *k* times with different groups as the training dataset and testing dataset, respectively. The average value of *k* times predicted accuracies is finally used as the evaluation indicator of forecasting performance. In this paper, the training dataset of the established database was utilised as the original data to conduct the *k*-CV operation on the machine learning models to obtain the evaluation indicator value (RMSE), with k being taken as 10 considering the size of database and the recommendation in literatures (Rodriguez et al., 2009). To compare the optimisation effects between MEA and traditional optimisation algorithms, the BPANN models with hyperparameters optimised by GA and PSO were constructed, respectively, and the predictive results of GA and PSO-BPANN model were compared with that of MEA-BPANN, respectively. The detailed introduction about the optimised hyperparameters of the built machine learning models and their optimising range is provided in Table 1.

4.Database and pre-processing

The research compiled the experimental data from about 4000 direct shear tests on clayey soil-geomembrane interfaces from the following sources: literature, internal database, repeatability testing, inter-laboratory comparison, own-laboratory experiments (Criley and Saint John, 1997; Dixon et al., 2006; Dixon et al., 2000; Sia and Dixon, 2007). The repeatability testing uses the same material in the same laboratory whereas the inter-laboratory testing uses the same material in different laboratories, and the internal database has both material and laboratory variability. The typical properties, such as density, mean particle size of clayey soil and roughness, density of geomembranes used in the tests were also complied. For other experimental conditions, the tests were the same, with a shearing rate of 1mm/min and being conducted in the consolidated undrained condition.

Among the 4000 direct shear tests, the tests that lack a complete set of information were excluded. The information of the remaining tests was compiled and arranged to construct the database with 623 data groups by combining the general soil classification standards and product data sheets of geomembrane manufacturers. The data groups were divided randomly into 498 groups of training data (80%) for training the machine-learning models and 125 groups of testing data (20%) for testing the trained machine-learning models by using a *MATLAB* program. In this program, each data group was randomly assigned a unique number ranging from 1 to 623. The data groups with number ranging from 1 to 498 were selected as the training dataset, and the data groups with number ranging from 498 to 623 were selected as the testing dataset. In each data group, soil density (D), soil mean particle size (M), geomembrane roughness (R), geomembrane density (G) , normal stress (N) were adopted as the input parameters for machine learning modelling, and the corresponding peak shear strength (S) of clayey soil-geomembrane interfaces was taken as the output parameter. The statistics parameters and data type of the input and output parameters were tabulated in Table 2.

The input parameters for the machine learning models had different dimensions, which may affect the training time and prediction accuracy of the models. To improve the forecasting accuracy and operational efficiency of the machine learning models, the input and output parameters were normalized to the range of 0–1 using Equation. (2).

$$x_{\text{Normalized}} = \frac{x - x_{\min}}{x_{\max} - x_{\min}} \tag{2}$$

Where, $x_{\text{Normalized}}$ represents the normalized value, x represents the original value, $x_{\min}$ represents the minimum value, and $x_{\max}$ represents the maximum value.

5. Quality assessment

Predictive precision of the established machine-learning models was assessed using three evaluation indicators: Correlation Coefficient R, RMSE, and Mean Absolute Percentage Error (MAPE), as expressed in Equation (3)~(5), respectively.

R is a statistic parameter that can measure the correlation between two variables, ranging from -1 to 1. A value of 1 means totally positive correlation, 0 means no correlation, and -1 means totally negative correlation.

$$R(f_i, y_i) = \frac{\operatorname{cov}(f_i, y_i)}{\sqrt{\operatorname{var}[f_i]\operatorname{var}[y_i]}} \tag{3}$$

Where, $\operatorname{cov}(,)$ represents covariance, $\operatorname{var}[\ ]$ represents variance, y_i represents the measured value (The value obtained in physical shear tests), $\bar{y}$ represents the average measured value, and f_i represents the predicted value.

RMSE is the standard deviation of estimation errors, which indicates how concentration the data is around the best fitting line. MAPE can measure the prediction accuracy as the form of percentage, and can be calculated as shown in Equation (4). The lower the RMSE and MAPE indicate the more precise the machine learning models.

$$\text{MSE} = \frac{|y_i - f_i|}{n} \tag{4}$$

Where, *n* represents the number of sample data.

$$MAPE = \frac{100\%}{n}\sum_{i=1}^{n}\frac{|y_i - f_i|}{y_i} \tag{5}$$

6.Results and analysis

6.1Results of hyperparameter optimisation

As aforementioned, MEA was utilised to optimise the hyperparameters of machine learning algorithms, with RMSE as fitness function. For each machine learning algorithm, three initial superior subgroups and three initial temporary subgroups were generated. The optimising process of the subgroups during the simillartaxis and dissimilation operations was recorded, as shown in Figure 2.

Based on Figure 2, for the initial superior subgroups and temporary subgroups, after serval similartaxis operations, the RMSE of each subgroup tends to be steady, which indicates the subgroups are mature. Then, the dissimilation operations are conducted. In the dissimilation operation, the RMSE of temporary subgroups and superior subgroups is compared, and the superior subgroups are replaced by the temporary subgroups with lower RMSE. The rest of temporary subgroups with high RMSE are abandoned, and individuals in them are released. After that, the released individuals are regrouped to form new temporary groups, and the similartaxis operations are performed again on the subgroups, as shown in Figure 2 (d). For the new superior subgroups, the RMSE of them remains stable because they are already mature, as shown in Figure 2 (c). By comparing the RMSE of new temporary subgroups and new superior subgroups, it can be seen that the RMSE of each superior subgroup is lower than that of temporary subgroup, which meets the ending criterion. Therefore, the subgroups do not need to be performed dissimilation operations again, and the corresponding hyperparameters of the center individual in the superior subgroup with the lowest RMSE are assigned as the initial parameters of the corresponding machine learning model.

Based on the aforementioned analysis, for most of subgroups, their RMSE reduces obviously and becomes stable within 15 iteration times. It indicates that MEA is efficient in the hyperparameters optimisation of the established machine learning models, which can enhance the predictive accuracy of established machine learning models remarkably with high efficiency.

To compare the optimisation effects between MEA and GA, PSO, the optimised processes of BPANN model using GA and PSO are shown in Figure 3, respectively.

As shown in Figure 2 and Figure 3, when MEA is adopted to optimise BPANN model, RMSE becomes stable within 18 times iterations, which is obviously lower than those of GA (80 times) and PSO (70 times), respectively. Additionally, after the optimisation of MEA, RMSE of BPANN model reduces to 4.69, while, for GA and PSO, they are 8.52 and 7.99, respectively. It demonstrates that, the optimisation performance of MEA on BPANN model is better than those of GA and PSO in the both aspects of optimising efficiency and increasing magnitude in predictive accuracy.

6.2 The performance of the developed machine learning models

The predictive performance of the established machine learning models on the training dataset and testing dataset is presented in Figure 4 to Figure 9, respectively.

Figure 4 to Figure 7 show that, for the training dataset, the forecasting performance of the ADABPANN model with hyperparameters optimized by MEA is the best among the constructed models in terms of the statistics parameters of R, RMSE and MAPE. More specifically, the MEA-ADABPANN model achieved the lowest RMSE (1.1) and MAPE (5.06%), and the highest R (0.99), among the models, followed by MEA-RF, MEA-BPANN and MEA-SVM, with GA-BPANN and PSO-BPANN having poor predictive accuracy.

As shown in Figure 6 to Figure 9, for the testing dataset, the ADABPANN model with hyperparameters optimized by MEA still has the highest foretelling precision among the models, with the lowest RMSE (1.26) and MAPE (6.56%), and the highest R (0.99), followed by MEA-RF, MEA-SVM and MEA-BPANN. The predictive performance of the GA-BPANN and PSO-BPANN are the worst among them.

The results indicate that, for both of testing dataset and training dataset, the ensemble algorithms of ADABPANN and RF have higher precision in estimating the peak shear strength of clayey soil-geomembrane interfaces than those of BPANN and SVM, respectively. Additionally, the models with hyperparameters optimized by MEA are more accurate to evaluate the peak shear strength than the models optimized by GA and PSO, respectively.

7. Sensitivity analysis of the influence factors

Sensitivity analysis was carried out to investigate the relative importance of the input parameters of the built machine learning models to the peak shear strength along clayey soil-geomembrane interfaces. Since the ADABPANN model with hyperparameters optimized by MEA was considered as the model with the highest predictive accuracy, the MEA-ADABPANN model was used to carried out the sensitivity analysis. Garson's Algorithm was utilized to calculate the relative importance of the input parameters for per BPANN model that composes the MEA-ADABPANN model (Goh, 1995), which has been extensively applied in geotechnical engineering to estimate the parameter contribution (Das and Basudhar, 2006; Goh, 1995; Kanungo et al., 2014). Garson's

Algorithm was proposed by Garson, later modified by Goh (1995), to determine the relative importance of the input parameters to the output parameter based on the connection weights of BPANN models, as shown in Equation (6). The average relative importance of the input parameters for each BPANN model in the MEA-ADABPANN model was calculated as the final relative importance, as presented in Figure 10.

$$R_{\mathrm{ij}} = \frac{\sum_{j=1}^{L}\left(\left|W_{ij}W_{jk}\right| / \sum_{r=1}^{N}\left|W_{rj}\right|\right)}{\sum_{i=1}^{N}\sum_{j=1}^{L}\left(\left|W_{ij}W_{jk}\right| / \sum_{r=1}^{N}\left|W_{rj}\right|\right)} \tag{6}$$

where R_{ij} is the relative importance of input parameters, W_{ij}, W_{jk} are the connection weights of the input layer-hidden layer and the hidden-output layer, i= 1,2….N , k=1,2….M (N and M are the numbers of the input parameters and output parameters).

Based on Figure 10, normal stress has the largest relative importance among the input parameters, accounting for 26.85 %, followed by soil density, geomembrane roughness and soil mean particle size. In comparison, geomembrane density has small influence on the peak shear strength.

8. Establishment of an analytical equation for estimating the peak shear strength

Based on the aforementioned analysis, the constructed ADABPANN model with hyperparameters optimized by MEA has been validated as a reliable tool to foretell the peak shear strength of clayey soil-geomembrane interfaces. However, owing to the complex modelling process, it is difficult for engineers with limited knowledge of machine learning to utilize the model. To facilitate the usage for geotechnical practitioners, an analytical equation based on the average weights and biases of the

BPANN models that compose the MEA-ADABPANN model was proposed by using Equation 7, with considering the predictive mechanism of MEA-ADABPANN model (Goh et al., 2005). The BPANN models in MEA-ADABPANN model have the same structure, with the average weights and biases of joints in the BPANN models are tabulated in Table 3. To be specific, the values in Table 3 include the average connection weights between the input layer joints and hidden layer joints, the average connection weights between the hidden layer joints and output layer joints, the biases of all joints. The similar equations established based on the same mechanism have been extensively adopted by researchers in the geotechnical area (Das and Basudhar, 2006; Goh, 1995; Kanungo et al., 2014), which has sufficiently validated the reliability of the equation.

$$Y_n = f_{sig}\{b_0 + \sum_{k=1}^{h}[w_k \times f_{sig}(b_{hk} + \sum_{i=1}^{m} w_{ik} X_i)]\} \quad (7)$$

Where, Y_n is the normalised predictive values in [-1,1]; b_0 is the average bias of output layer joints; w_k is the average connection weight between the *k*th hidden layer joint and the output layer joint; b_{hk} is the average bias of the *k*th hidden layer joint; *h* is the number of hidden layer joints; w_{ik} is the average connection weight between the *i*th input layer joint and the *k*th hidden layer joint; X_i is the *i*th normalised input parameter, ranging from -1 to 1; f_{sig} is the Sigmoid Transfer Activation Function; *m* is the number of input layer joints.

The detailed calculation process is follows, with the input parameters and output parameter represented by their corresponding symbols, respectively:

$$A_1 = 2.22 + 3.37R + 0.11D - 2.26M + 2.2G + 0.19N \quad (8)$$

$$A_2 = -1.55 + 0.08R + 0.06D - 0.01M + 2.32G + 1.12N \quad (9)$$

$$A_3 = -1.94 - 2.94R - 0.09D + 2.18M + 2.21G - 0.65N \tag{10}$$

$$A_4 = -0.6 - 0.09R - 0.05D + 0.1M + 0.19G + 0.06N \tag{11}$$

$$A_5 = -3.48 - 0.04R - 0.0004D + 0.018M + 0.01G - 1.29N \tag{12}$$

$$A_6 = 2.08 - 2.34R - 0.35D + 0.72M - 0.14G - 0.02N \tag{13}$$

$$A_7 = -0.29 - 1.43R - 2.02D - 2.81M + 1.16G + 0.07N \tag{14}$$

$$A_8 = -0.09 - 2.26R + 0.52D - 0.01M - 0.09G - 2.91N \tag{15}$$

$$A_9 = 1.56 - 1.61R - 0.29D + 0.47M - 1.19G + 2.19N \tag{16}$$

$$B_1 = 1.1 \times \frac{e^{A_1} - e^{-A_1}}{e^{A_1} + e^{-A_1}} \tag{17}$$

$$B_2 = -5.38 \times \frac{e^{A_2} - e^{-A_2}}{e^{A_2} + e^{-A_2}} \tag{18}$$

$$B_3 = 1.19 \times \frac{e^{A_3} - e^{-A_3}}{e^{A_3} + e^{-A_3}} \tag{19}$$

$$B_4 = 0.95 \times \frac{e^{A_4} - e^{-A_4}}{e^{A_4} + e^{-A_4}} \tag{20}$$

$$B_5 = 2.56 \times \frac{e^{A_5} - e^{-A_5}}{e^{A_5} + e^{-A_5}} \tag{21}$$

$$B_6 = 0.79 \times \frac{e^{A_6} - e^{-A_6}}{e^{A_6} + e^{-A_6}} \tag{22}$$

$$B_7 = 0.05 \times \frac{e^{A_7} - e^{-A_7}}{e^{A_7} + e^{-A_7}} \tag{23}$$

$$B_8 = 0.08 \times \frac{e^{A_8} - e^{-A_8}}{e^{A_8} + e^{-A_8}} \tag{24}$$

$$B_9 = -1.22 \times \frac{e^{A_9} - e^{-A_9}}{e^{A_9} + e^{-A_9}} \tag{25}$$

$$C_1 = -2.3 + B_1 + B_2 + B_3 + B_4 + B_5 + B_6 + B_7 + B_8 + B_9 \quad (26)$$

$$Y_n = \frac{e^{C_1} - e^{-C_1}}{e^{C_1} + e^{-C_1}} \quad (27)$$

Among the above equations, A, B, C, Yn are just a symbol, which represents the corresponding equations. The relationship between Equation (8)~(27) is as follows: Equation (8)~(16) indicate the definition of A_1 to A_9. Then, A_1 to A_9 are substituted into Equation (17)~(25) to definite B_1 to B_9, respectively. After that, B_1 to B_9 are substituted into Equation (26) to definite C_1. Followed that, C_1 is substituted into Equation (27) to definite Yn. Finally, since the obtained Y_n value from Equation (27) is in the range of [-1,1], Yn is substituted into Equation (28) to conduct denormalization to obtain the forecasting peak shear strength of clayey soil-geomembrane interfaces.

$$\tau = 0.5(Y_n + 1)(Y_{\max} - Y_{\min}) + Y_{\min} \quad (28)$$

Where, $Y_{\max}$ and $Y_{\min}$ are the maximum and minimum values of the peak shear strength in the database, respectively, in this research, $Y_{\max} = 90kPa$ and $Y_{\min} = 5kPa$.

Therefore, Equation (28) is transformed to Equation (29) to obtain the empirical equation for calculating the peak shear strength. By using Equation (29) can achieve the prediction of the peak shear strength of clayey soil-geomembrane interfaces without conducting the MEA-ADABPANN modelling steps. The relevant practitioners can apply Equation (29) in forecasting the peak shear strength based on the parameters listed in Table 2.

$$\tau = 42.5kPa \times Y_n + 47.5kPa \quad (29)$$

9. Validation by conducting physical experiments

To validate the effectiveness of the developed analytical equation, physical direct shear tests on clayey soil-geomembrane interfaces were conducted by using the bespoke soil-geosynthetics interface large direct shear apparatus in the geotechnical laboratory at Shanghai Maritime University, China, as shown in Figure 11. In the tests, two types of clayey soil and 6 types of geomembranes, with different properties, were adopted, as listed in Table 4 and Table 5. The normal pressure was set as 50 kPa, 100 kPa and 150kPa, respectively, and the shearing was implemented in the consolidated undrained condition, with shearing rate of 1 mm/min. In total, 36 tests were carried out. According to the experimental results, the peak shear strength along the interfaces between different types of clayey soil and geomembrane was obtained. Also, the developed empirical equation (Equation (28)) was adopted to predict the peak shear strength along the interfaces between clayey soil and geomembranes with different properties. By comparing the measured peak shear strength and the predicted value, the applicability of the developed equation is verified. The comparison results are shown in Figure 12.

As shown in Figure 12, the predicted peak shear strength is close to the peak shear strength measured by laboratory tests, with R of 0.98, RMSE of 1,20 and MAPE of 4.5%. This indicates that the developed equation has high accuracy to predict the peak shear strength of clayey soil-geomembrane interfaces. It provides convenience for the geotechnical engineering personnel with limited knowledge of machine learning technique to forecast the peak shear strength of clayey soil-geomembrane interfaces.

10. Discussion

In practical engineering, the moisture content of soil has relatively large influence on the peak shear strength of clayey soil-geomembrane interfaces. Due to the lack of relevant information about the moisture content of clayey soil in the compiled database, the proposed machine learning models in this research do not employ the soil moisture content as one of input parameters. However, the developed machine learning models without the input parameter of soil moisture content still have satisfactory predictive results. The possible explanation is that, based on the standard procedure of conducting large direct shear tests on soil-geosynthetics interfaces (ASTM, 2014), the direct shear tests are normally carried out on the interfaces between clayey soil with the optimum moisture content and geomembrane. For clayey soil, their optimum moisture content is close. Thus, it is supposed that, in the compiled database, the moisture content of clayey soil adopted in different direct shear tests is similar, which leads to that the presented machine learning models can have good forecasting outcomes without the input parameter of soil moisture content.

In this research, the forecasting performance of the MEA tuned ADABPANN model is the best among the established models. It can be attributed to the four reasons. (i) MEA can divide the subgroups into superior and temporary subgroups, with the similartaxis and dissimilation operations being conducted independently, which can significantly increase the search efficiency for the optimal solution. (ii) MEA can record more than one generation of evolutionary information, which can provide correct guidance on the direction of similartaxis and dissimilation operations. (iii) Similartaxis and dissimilation operations in MEA can avoid the destruction of original individual caused by the crossover and mutation operations in GA. (iv) MEA tuned ADABPANN can achieve both of the strong local and global searching capability to determine the optimal solution, which can avoid premature convergence and poor prediction effect to obtain better forecasting precision.

11. Limitations

Although some significant discoveries have been revealed in this paper, the limitation of the investigation should not be ignored. Firstly, the predictive precision and reliability of the constructed machine learning models can be improved further when a larger database is available. Secondly, the established machine learning models were based on the database developed from the large direct shear tests on the interfaces between clayey soil and geomembrane. In the future, it is worthy expanding the database to include the data from the tests on the interfaces between different types of soil and geomembrane. Thirdly, the value ranges of some input parameters, such as soil mean particle size and geomembrane density, are not very large, Hence, an attempt to expand the value ranges of the input parameters is deserved to carry out, to improve the generalisation ability of the established machine learning models.

12 Conclusion

In the present research, based on the database constructed upon the 623 large direct shear tests on clayey soil-geomembrane interfaces, a novel machine learning model was established by combining MEA and ADA-BPANN to estimate the peak shear strength of clayey soil-geomembrane interfaces according to the 5 input variables of soil density (D), soil mean particle size (M), geomembrane roughness (R), geomembrane density (G) and normal stress (N). To validate the performance of the novel machine learning model, the conventional machine learning algorithms including GA and PSO tuned ADA-BPANN, MEA tuned ELM and RF models were established to compare with the MEA tuned ADA-BPANN model. Also, the sensitivity analysis was implemented to determine the influence degree of input variables to the peak shear strength, and an analytical equation was proposed to facilitate the prediction of peak shear strength for geotechnical engineering practitioners with limited machine learning knowledge.

The research outcomes indicate that the proposed novel machine learning combined by MEA and ADA-BPANN has better prediction performance than the others machine learning models. To be specific, the MEA tuned ADA-BPANN model has higher predicting accuracy and efficiency, less iteration times to reach the optimal solution, less possibility of over-fitting and trapping into local optima, compared to the conventional algorithms. Also, the sensitivity analysis upon the proposed model manifests that the impact of normal stress on the peak shear strength is the highest, being followed by soil density and geomembrane roughness. It provides a guidance for the relevant practitioners to pay more attention on the factors that have more significant influence on the peak shear strength of clayey soil-geomembrane interfaces.

Overall, although evaluating the peak shear strength of clayey soil-geomembrane interfaces is always a large challenge due to the multiple influence factors and complicated action mechanism, the novel machine learning model presented in this research provides a possibility to preciously forecast the peak shear strength, with a high efficiency. It also acts as a key solution to overcome the deficiencies and uncertainties about the design of building that requires the correct estimation of the peak shear strength for clayey soil-geomembrane interfaces.

Acknowledgements

The authors would like to acknowledge the consistent support of 2022 Open Project of Failure Mechanics and Engineering Disaster Prevention, Key Lab of Sichuan Province, No FMEDP202209. The paper is also sponsored by Shanghai Sailing Program, No 22YF1415800

Reference

Abad, A.R.B., Ghorbani, H., Mohamadian, N., Davoodi, S., Mehrad, M., Aghdam, S.K.Y., Nasriani, H.R., 2022. Robust hybrid machine learning algorithms for gas flow rates prediction through wellhead chokes in gas condensate fields. Fuel 308, 121872.

Abdelaal, F., Morsy, M., Rowe, R.K., 2019. Long-term performance of a HDPE geomembrane stabilized with HALS in chlorinated water. Geotextiles and Geomembranes 47 (6), 815-830.

Abdelaal, F., Solanki, R., 2022. Effect of geotextile ageing and geomembrane surface roughness on the geomembrane-geotextile interfaces for heap leaching applications. Geotextiles and Geomembranes 50 (1), 55-68.

Ahmadi, M.A., Chen, Z., 2019. Comparison of machine learning methods for estimating permeability and porosity of oil reservoirs via petro-physical logs. Petroleum 5 (3), 271-284.

Al-Mudhafar, W.J., 2017. Integrating well log interpretations for lithofacies classification and permeability modeling through advanced machine learning algorithms. Journal of Petroleum Exploration and Production Technology 7 (4), 1023-1033.

Al Khalifah, H., Glover, P., Lorinczi, P., 2020. Permeability prediction and diagenesis in tight carbonates using machine learning techniques. Marine and Petroleum Geology 112, 104096.

Asteris, P.G., Koopialipoor, M., Armaghani, D.J., Kotsonis, E.A., Lourenço, P.B., 2021. Prediction of cement-based mortars compressive strength using machine learning techniques. Neural Computing and Applications 33 (19), 13089-13121.

ASTM, 2014. Standard test method for determining the shear strength of soil-geosynthetic and geosynthetic-geosynthetic interfaces by direct shear. Annual Book of ASTM Standards. ASTM D5321, West Conshohocken, PA.

Biabani, M.M., Indraratna, B., 2015. An evaluation of the interface behaviour of rail subballast stabilised with geogrids and geomembranes. Geotextiles and Geomembranes 43 (3), 240-249.

Çalışkan, A., Demirhan, S., Tekin, R., 2022. Comparison of different machine learning methods for estimating compressive strength of mortars. Construction and Building Materials 335, 127490.

Cazzuffi, D., Gioffrè, D., 2020. Lifetime assessment of exposed PVC-P geomembranes installed on Italian dams. Geotextiles and Geomembranes 48 (2), 130-136.

Chao, Z., Fowmes, G., 2021. Modified stress and temperature-controlled direct shear apparatus on soil-geosynthetics interfaces. Geotextiles and Geomembranes 49 (3), 825-841.

Chao, Z., Fowmes, G., 2022. The short-term and creep mechanical behaviour of clayey soil-geocomposite drainage layer interfaces subjected to environmental loadings. Geotextiles and Geomembranes 50 (2), 238-248.

Chao, Z., Fowmes, G., Dassanayake, S., 2021. Comparative study of hybrid artificial intelligence approaches for predicting peak shear strength along soil-geocomposite drainage layer interfaces. International Journal of Geosynthetics and Ground Engineering 7 (3), 1-19.

Chao, Z., Wang, M., Sun, Y., Xu, X., Yue, W., Yang, C., Hu, T., 2022. Predicting stressdependent gas permeability of cement mortar with different relative moisture contents based on hybrid ensemble artificial intelligence algorithms. Construction and Building Materials 348, 128660.

Chen, W.B., Xu, T., Zhou, W.H., 2021. Microanalysis of smooth geomembrane–sand interface using FDM–DEM coupling simulation. Geotextiles and Geomembranes 49 (1), 276-288.

Choubineh, A., Ghorbani, H., Wood, D.A., Moosavi, S.R., Khalafi, E., Sadatshojaei, E., 2017. Improved predictions of wellhead choke liquid critical-flow rates: modelling based on hybrid neural network training learning based optimization. Fuel 207, 547-560.

Criley, K., Saint, J.D., 1997. Variability analysis of soil vs. geosynthetic interface friction characteristics by multiple direct shear testing. In: Proceedings of Geosynthetics. Long Beach, USA, pp. 885-897.

Das, S.K., Basudhar, P.K., 2006. Undrained lateral load capacity of piles in clay using artificial neural network. Computers and Geotechnics 33 (8), 454-459.

Debnath, P., Dey, A.K., 2017. Prediction of laboratory peak shear stress along the cohesive soil–geosynthetic interface using artificial neural network. Geotechnical and Geological Engineering 35 (1), 445-461.

Dixon, N., Jones, D.R.V., Fowmes, G.J., 2006. Interface shear strength variability and its use in reliability-based landfill stability analysis. Geosynthetics International 13 (1), 1-14.

Dixon, N., Kamugisha, P., Jones, D., 2000. Geosynthetic interface testing at low normal stresses: design implications. In: Proceedings of the Second European Geosynthetics Conference. Bologna, Italy, pp. 535-540.

Ebrahimi, E., Monjezi, M., Khalesi, M.R., Armaghani, D.J., 2016. Prediction and optimization of back-break and rock fragmentation using an artificial neural network and a bee colony algorithm. Bulletin of Engineering Geology and the Environment 75 (1), 27-36.

Eldesouky, H., Brachman, R., 2018. Calculating local geomembrane strains from a single gravel particle with thin plate theory. Geotextiles and Geomembranes 46 (1), 101-110.

Eldesouky, H., Brachman, R., 2020. Viscoplastic modelling of HDPE geomembrane local stresses and strains. Geotextiles and Geomembranes 48 (1), 41-51.

Erofeev, A., Orlov, D., Ryzhov, A., Koroteev, D., 2019. Prediction of porosity and permeability alteration based on machine learning algorithms. Transport in Porous Media 128 (2), 677-700.

Ghazavi, M., Bavandpouri, O., 2022. Analytical solution for calculation of pull out force-deformation of geosynthetics reinforcing unsaturated soils. Geotextiles and Geomembranes 50 (2), 357-369.

Ghazizadeh, S., Bareither, C.A., 2018. Stress-controlled direct shear testing of geosynthetic clay liners II: assessment of shear behavior. Geotextiles and Geomembranes 46 (5), 667-677.

Ghorbani, H., Moghadasi, J., Wood, D.A., 2017. Prediction of gas flow rates from gas condensate reservoirs through wellhead chokes using a firefly optimization algorithm. Journal of Natural Gas Science and Engineering 45, 256-271.

Goh, A.T., 1995. Back-propagation neural networks for modeling complex systems. Artificial Intelligence in Engineering 9 (3), 143-151.

Goh, A.T., Kulhawy, F.H., Chua, C., 2005. Bayesian neural network analysis of undrained side resistance of drilled shafts. Journal of geotechnical and

geoenvironmental engineering 131 (1), 84-93.
Hasanipanah, M., Amnieh, H.B., Arab, H., Zamzam, M.S., 2018. Feasibility of PSO–ANFIS model to estimate rock fragmentation produced by mine blasting. Neural Computing and Applications 30 (4), 1015-1024.
He, P.F., Mu, Y.H., Ma, W., Huang, Y.T., Dong, J.H., 2021. Testing and modeling of frozen clay–concrete interface behavior based on large-scale shear tests. Advances in Climate Change Research 12 (1), 83-94.
He, Z., Mo, H., Siga, A., Zou, J., 2019. Research on the parameters of nonlinear hyperbolic model for clay-geogrid interfaces based on large scale direct shear tests. Transportation Geotechnics 18, 39-45.
Jie, J., Zeng, J., Ren, Y., 2004. Improved mind evolutionary computation for optimizations. In: Fifth World Congress on Intelligent Control and Automation (Cat. No. 04EX788). Hangzhou, China, pp. 2200-2204.
Kanungo, D., Sharma, S., Pain, A., 2014. Artificial neural network (ANN) and regression tree (CART) applications for the indirect estimation of unsaturated soil shear strength parameters. Frontiers of Earth Science 8 (3), 439-456.
Koerner, G., Koerner, R., 2006. Long-term temperature monitoring of geomembranes at dry and wet landfills. Geotextiles and Geomembranes 24 (1), 72-77.
Kohestani, V., Hassanlourad, M., Ardakani, A., 2015. Evaluation of liquefaction potential based on CPT data using random forest. Natural Hazards 79 (2), 1079-1089.
Kumar, S., Basudhar, P.K., 2018. A neural network model for slope stability computations. Géotechnique Letters 8 (2), 149-154.
Liaw, A., Wiener, M., 2002. Classification and regression by randomForest. R news 2 (3), 18-22.
Liu, C.N., Ho, Y.H., Huang, J.W., 2009. Large scale direct shear tests of soil/PET-yarn geogrid interfaces. Geotextiles and Geomembranes 27 (1), 19-30.
Liu, H., Tian, H., Liang, X., Li, Y., 2015. New wind speed forecasting approaches using fast ensemble empirical model decomposition, genetic algorithm, mind evolutionary algorithm and artificial neural networks. Renewable Energy 83, 1066-1075.
Lopes, M.L., Ferreira, F., Carneiro, J.R., Vieira, C.S., 2014. Soil–geosynthetic inclined plane shear behavior: influence of soil moisture content and geosynthetic type. International Journal of Geotechnical Engineering 8 (3), 335-342.
Makkar, F.M., Chandrakaran, S., Sankar, N., 2017. Performance of 3-D geogrid-reinforced sand under direct shear mode. International Journal of Geotechnical Engineering, 1-9.
Mehrjardi, G.T., Motarjemi, F., 2018. Interfacial properties of geocell-reinforced granular soils. Geotextiles and Geomembranes 46 (4), 384-395.
Mirzababaei, M., Arulrajah, A., Horpibulsuk, S., Aldava, M., 2017. Shear strength of a fibre-reinforced clay at large shear displacement when subjected to different stress histories. Geotextiles and Geomembranes 45 (5), 422-429.
Pant, A., Ramana, G., 2022. Prediction of pullout interaction coefficient of geogrids by extreme gradient boosting model. Geotextiles and Geomembranes.
Punetha, P., Mohanty, P., Samanta, M., 2017. Microstructural investigation on mechanical behavior of soil-geosynthetic interface in direct shear test. Geotextiles and Geomembranes 45 (3), 197-210.
Raja, M.N.A., Shukla, S.K., 2020. Ultimate bearing capacity of strip footing resting on soil bed strengthened by wraparound geosynthetic reinforcement technique. Geotextiles and Geomembranes 48 (6), 867-874.
Raja, M.N.A., Shukla, S.K., 2021. Predicting the settlement of geosynthetic-reinforced

soil foundations using evolutionary artificial intelligence technique. Geotextiles and Geomembranes 49 (5), 1280-1293.

Rodriguez, J.D., Perez, A., Lozano, J.A., 2009. Sensitivity analysis of k-fold cross validation in prediction error estimation. IEEE transactions on pattern analysis and machine intelligence 32 (3), 569-575.

Rowe, R., Rimal, S., Sangam, H., 2009. Ageing of HDPE geomembrane exposed to air, water and leachate at different temperatures. Geotextiles and Geomembranes 27 (2), 137-151.

Rowe, R.K., Jabin, F., 2021. Effect of prehydration, permeant, and desiccation on GCL/Geomembrane interface transmissivity. Geotextiles and Geomembranes 49 (6), 1451-1469.

Rowe, R.K., Shoaib, M., 2017. Long-term performance of high-density polyethylene (HDPE) geomembrane seams in municipal solid waste (MSW) leachate. Canadian Geotechnical Journal 54 (12), 1623-1636.

Saghatforoush, A., Monjezi, M., Faradonbeh, R.S., Armaghani, D.J., 2016. Combination of neural network and ant colony optimization algorithms for prediction and optimization of flyrock and back-break induced by blasting. Engineering with Computers 32 (2), 255-266.

Sathyan, D., Govind, D., Rajesh, C., Gopikrishnan, K., Kannan, G.A., Mahadevan, J., 2020. Modelling the shear flow behaviour of cement paste using machine learning-XGBoost. In: Journal of Physics: Conference Series. Telangana, India, 1451 (1), pp. 012026.

Sharma, J., Fleming, I., Jogi, M., 2007. Measurement of unsaturated soil–geomembrane interface shear-strength parameters. Canadian Geotechnical Journal 44 (1), 78-88.

Shen, J., Li, L., Lin, D., 2020. Prediction of engineering parameters based on improved artificial neural network. In: IE&EM 2019. Springer, Singapore, pp. 21-27.

Sia, A., Dixon, N., 2007. Distribution and variability of interface shear strength and derived parameters. Geotextiles and Geomembranes 25 (3), 139-154.

Sudakov, O., Burnaev, E., Koroteev, D., 2019. Driving digital rock towards machine learning: predicting permeability with gradient boosting and deep neural networks. Computers & geosciences 127, 91-98.

Sun, C., Yan, S., Xie, K., 2000. Mind-evolution-based machine learning and applications. In: Proceedings of the 3rd World Congress on Intelligent Control and Automation (Cat. No. 00EX393). Hefei, China, pp. 112-117.

Suzuki, M., Koyama, A., Kochi, Y., Urabe, T., 2017. Interface shear strength between geosynthetic clay liner and covering soil on the embankment of an irrigation pond and stability evaluation of its widened sections. Soils and Foundations 57 (2), 301-314.

Vangla, P., Gali, M.L., 2016. Shear behavior of sand-smooth geomembrane interfaces through micro-topographical analysis. Geotextiles and Geomembranes 44 (4), 592-603.

Wang, H., Shen, J., 2018. An improved model combining evolutionary algorithm and neural networks for PV maximum power point tracking. IEEE Access 7, 2823-2827.

Wang, W., Tang, R., Li, C., Liu, P., Luo, L., 2018. A BP neural network model optimized by mind evolutionary algorithm for predicting the ocean wave heights. Ocean Engineering 162, 98-107.

Wang, X., An, S., Xu, Y., Hou, H., Chen, F., Yang, Y., Zhang, S., Liu, R., 2019. A back propagation neural network model optimized by mind evolutionary algorithm for estimating Cd, Cr, and Pb concentrations in soils using Vis-NIR diffuse reflectance spectroscopy. Applied Sciences 10 (1), 51.

Xie, K., Du, Y., Sun, C., 2000. Application of the mind-evolution-based machine learning in mixture-ratio calculation of raw materials cement. In: Proceedings of the 3rd World Congress on Intelligent Control and Automation (Cat. No. 00EX393). Hefei, China, pp. 132-134.

Xu, L., Du, X., Wang, B., 2018. Short-term traffic flow prediction model of wavelet neural network based on mind evolutionary algorithm. International Journal of Pattern Recognition and Artificial Intelligence 32 (12), 1850041.

Yao, B.Z., Yang, C.Y., Yao, J.B., Sun, J., 2010. Tunnel surrounding rock displacement prediction using support vector machine. International Journal of Computational Intelligence Systems 3 (6), 843-852.

Yu, Y., Rowe, R.K., 2018. Development of geomembrane strains in waste containment facility liners with waste settlement. Geotextiles and Geomembranes 46 (2), 226-242.

Zhang, J., Li, P., Yin, X., Wang, S., Zhu, Y., 2022. Back analysis of surrounding rock parameters in pingdingshan mine based on bp neural network integrated mind evolutionary algorithm. Mathematics 10 (10), 1746.

Zhao, Y., Ren, X., Hu, Y., Wang, J., Bao, X., 2016. CNC thermal compensation based on mind evolutionary algorithm optimized BP neural network. World Journal of Engineering and Technology 4 (01), 38.

List of tables

Table.1 The optimised hyperparameters in the machine learning models

Machine learning models	Hyperparameter	Optimising range
BPANN	The initial weights of joints	-5-5
	The initial thresholds of joints	-10-10
SVM	Penalty parameter c of kernel function	2^{-5}-2^{5}
	Penalty parameter g of kernel function	4^{-5}-4^{5}
ADA-BPANN	The number of base learners	1-20
	The initial weights of joints in base learners	-5-5
	The initial threshold of joints in base learners	-10-10
RF	The maximum number of DT in the ensemble model	1-1000
	The minimum number of samples at the leaf node	1-10

Table. 2 The statistical characteristics of the established database

Parameters	Categorise	Data type	Minimum	Maximum	Mean
Soil mean particle size /mm	Input parameter	Numeric	0.001	0.05	0.02
Soil density/ g/cm^3	Input parameter	Numeric	1	1.7	1.4
Geomembrane roughness	Input parameter	Nominal	Smooth, Textured		
Geomembrane density/g/cm^3	Input parameter	Numeric	0.5	4	2
Normal pressure/kPa	Input parameter	Numeric	10	200	100
Peak shear strength/kPa	Output parameter	Numeric	5	90	50

Table.3 Average connection weights and biases of the MEA-ADABPNN models

Hidden Joint number	Weights						Biases	
	Input parameters					Output parameter	Hidden Layer	Output Layer
	R	*D*	*M*	*G*	*N*	*S*		
1	3.37	0.11	-2.26	2.2	0.19	1.10	2.22	
2	0.08	0.06	-0.01	2.32	1.12	-5.38	-1.55	
3	-2.94	-0.09	2.18	2.21	-0.65	1.19	-1.94	
4	-0.09	-0.05	0.10	0.19	0.06	0.95	-0.60	
5	-0.04	-0.0004	0.018	0.01	-1.29	2.56	-3.48	-2.30
6	-2.34	-0.35	0.72	-0.14	-0.02	0.79	2.08	
7	-1.43	-2.02	-2.81	1.16	0.07	0.05	-0.29	
8	-2.26	0.52	-0.01	-0.09	-2.91	0.08	-0.09	
9	-1.61	-0.29	0.47	-1.19	2.19	-1.22	1.56	

Table 4. The basic properties of clayey soil

Soil type	Soil density	Soil mean particle size/mm
Kaolin Clay	1.5	0.006
Bentonite Clay	1.2	0.04

Table 5. The basic properties of geomembranes

Geomembrane type	Geomembrane roughness	Geomembrane density/g/cm3
Geomembrane A	Smooth	1
Geomembrane B	Smooth	1.5
Geomembrane C	Smooth	3.9
Geomembrane D	Textured	1.5
Geomembrane E	Textured	2.9
Geomembrane F	Textured	4

List of figures

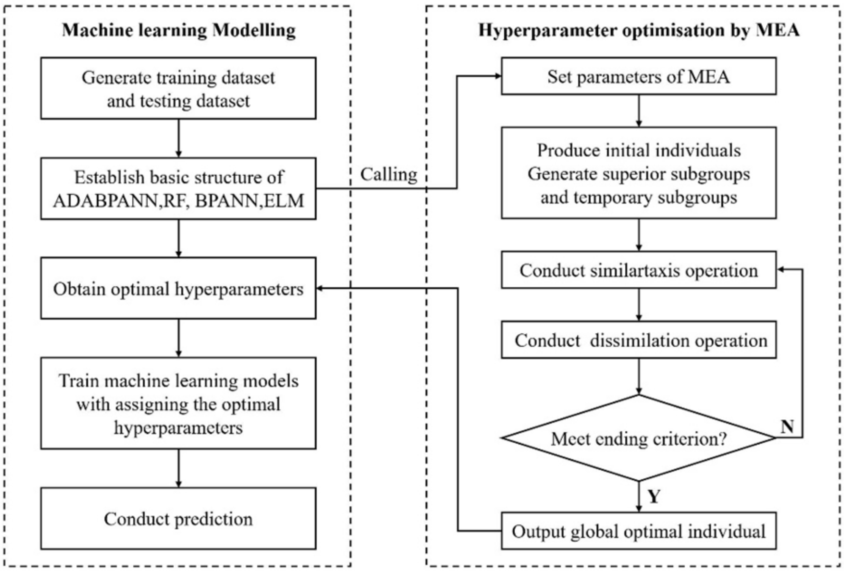

Figure.1 The flow chart of machine learning modelling with MEA optimised

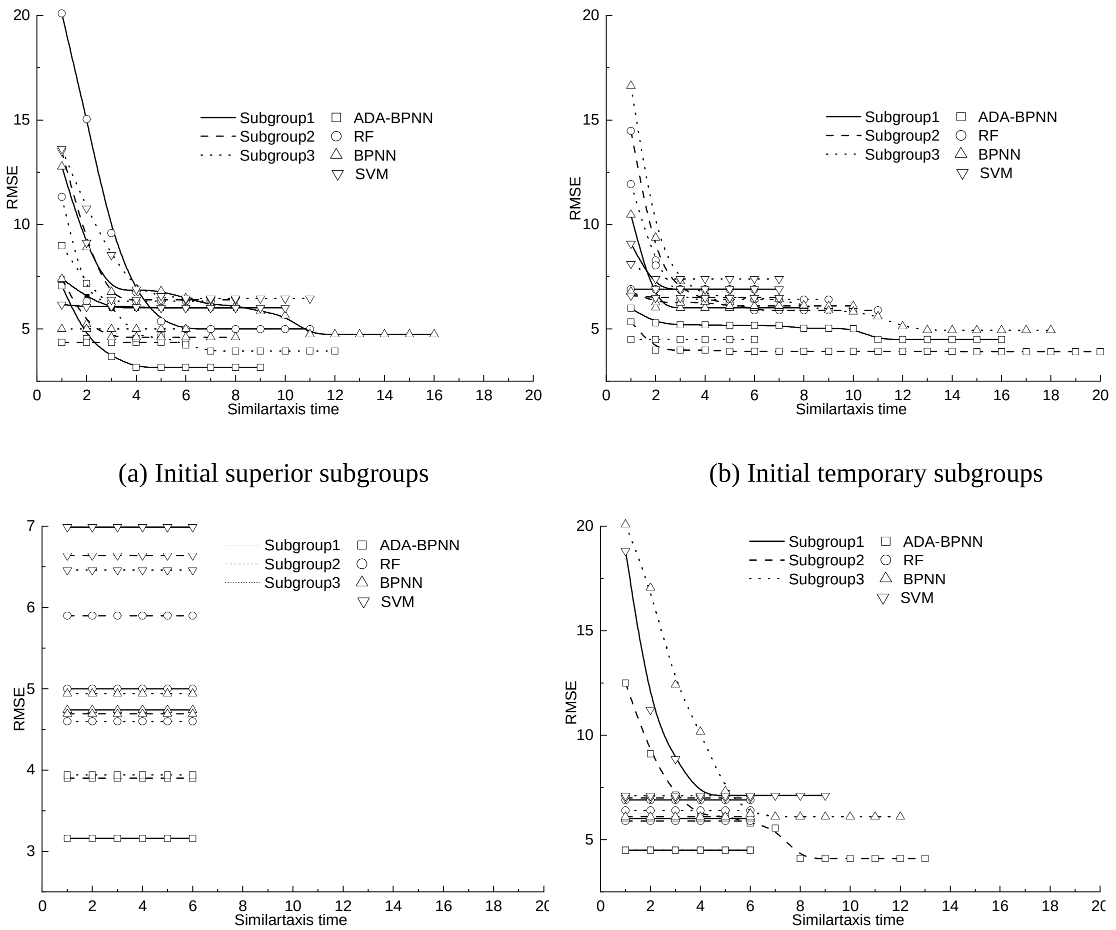

(a) Initial superior subgroups (b) Initial temporary subgroups

(c) Superior subgroups after dissimilation operation (d) Temporary subgroups after dissimilation operation

Figure.2 The evolution of RMSE during similartaxis process

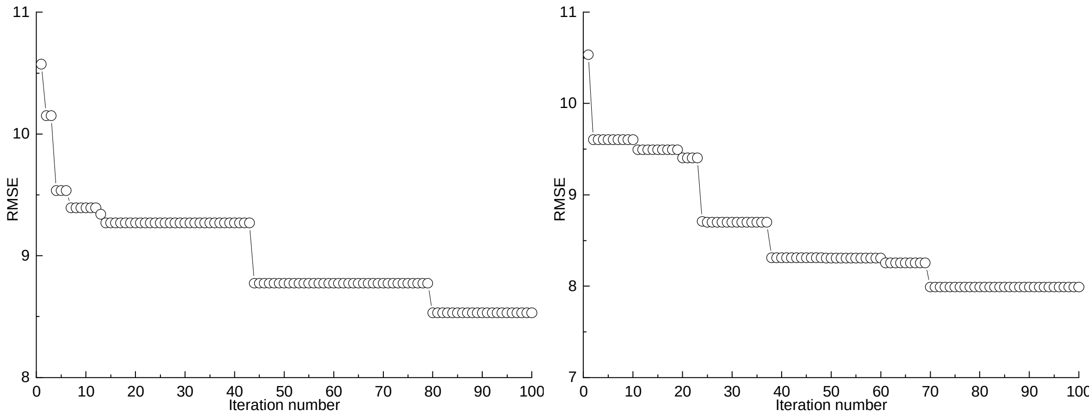

(a)GA-BPANN (b)PSO-BPANN

Figure.3 The optimised processes of BPANN models using GA and PSO

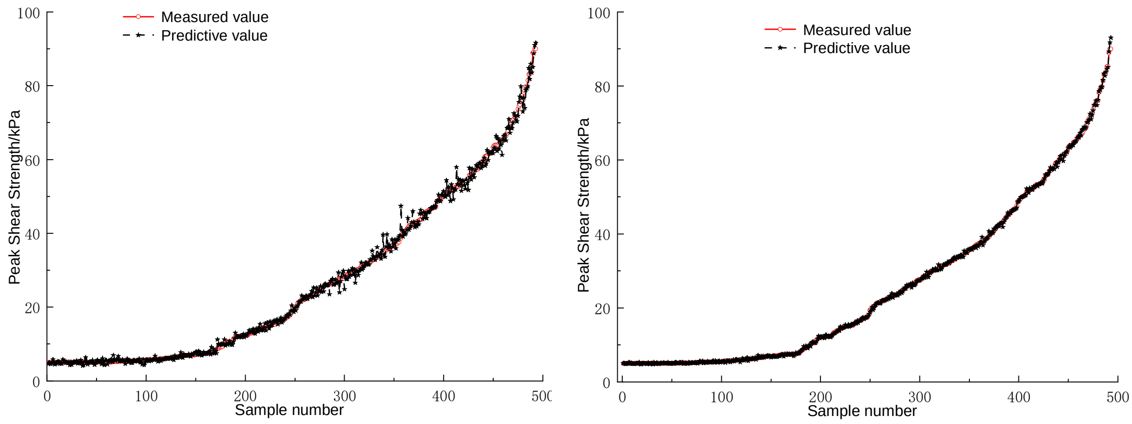

(a)MEA-BPANN (b)MEA-ADABAPNN

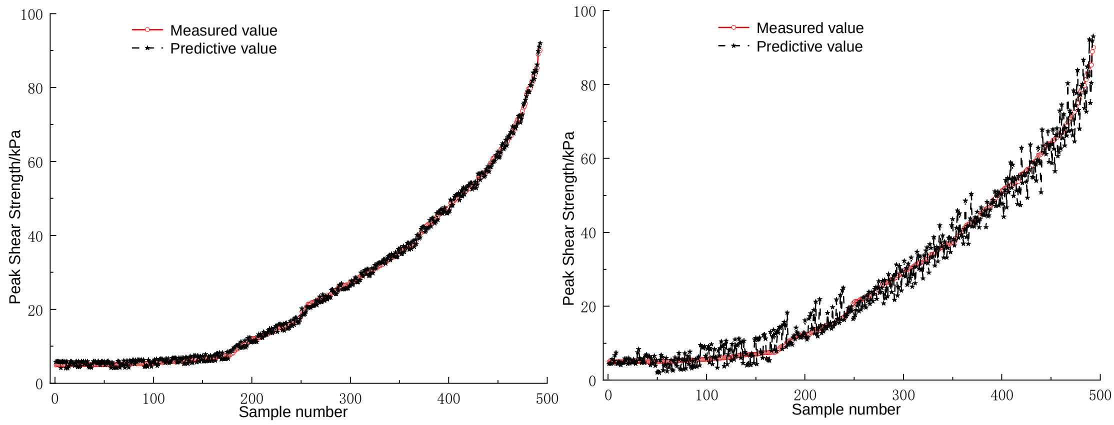

(c) MEA-RF (d) MEA-SVM

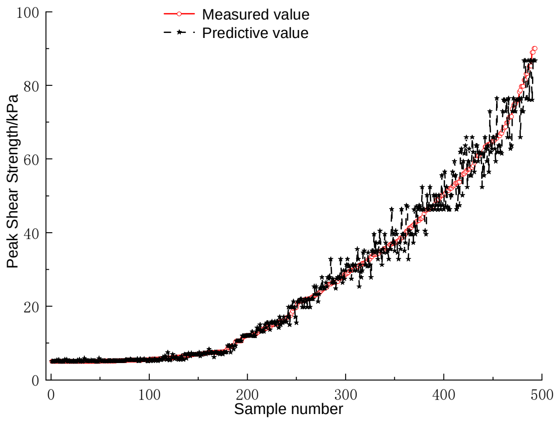

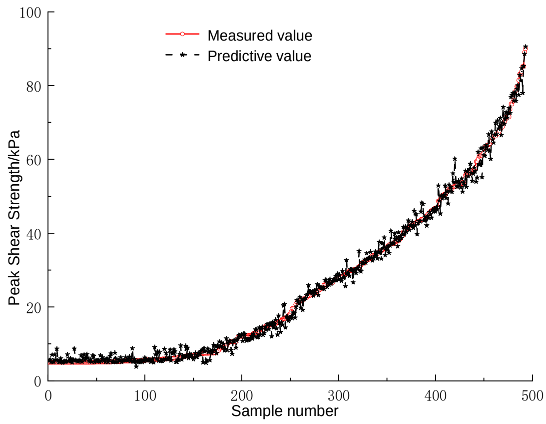

(e)GA-BPNN (f) PSO-BPNN

Figure.4 Predictive performance of the models for training dataset

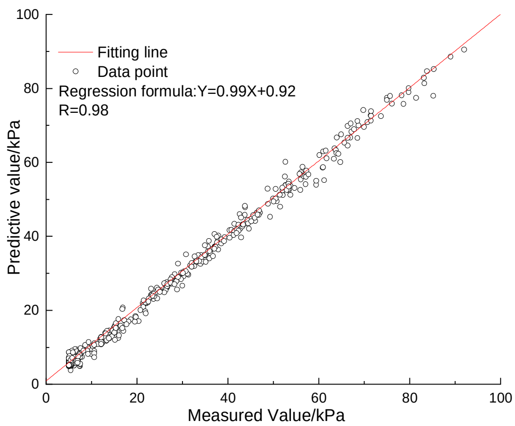

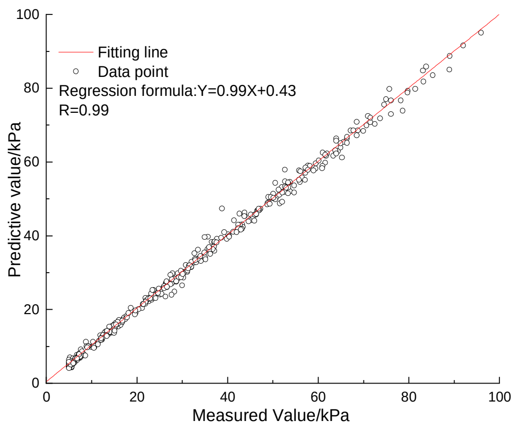

(a)MEA-BPANN (b)MEA-ADABPNN

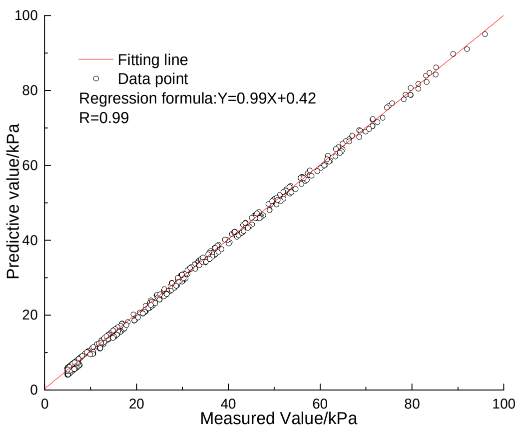

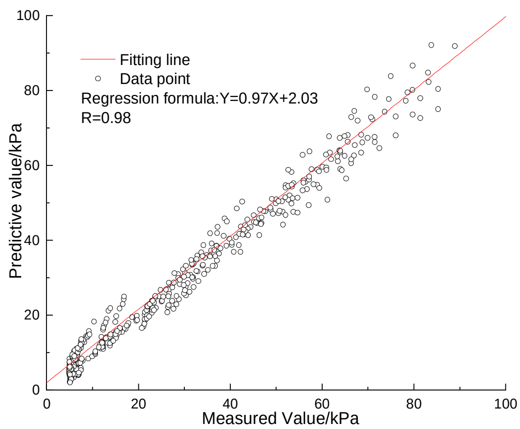

(c) MEA-RF (d) MEA-SVM

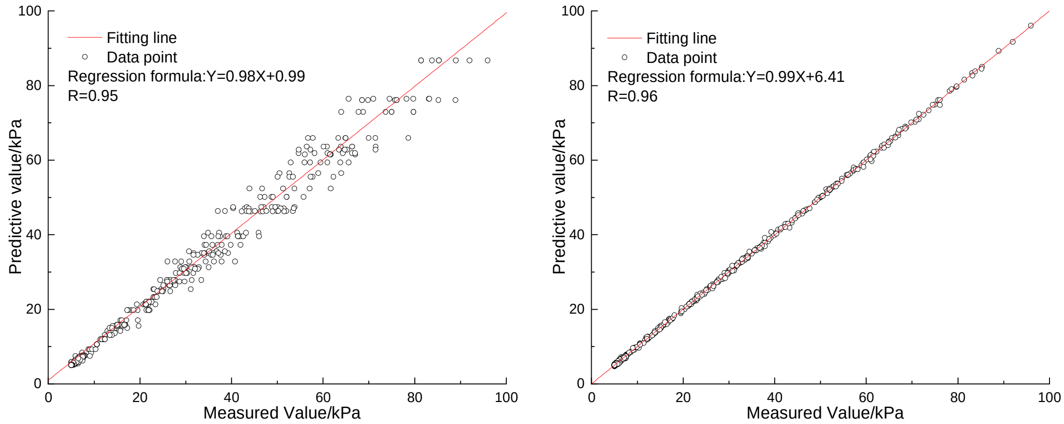

(e)GA-BPNN (f) PSO-BPNN

Figure.5 The R values of the models for training dataset

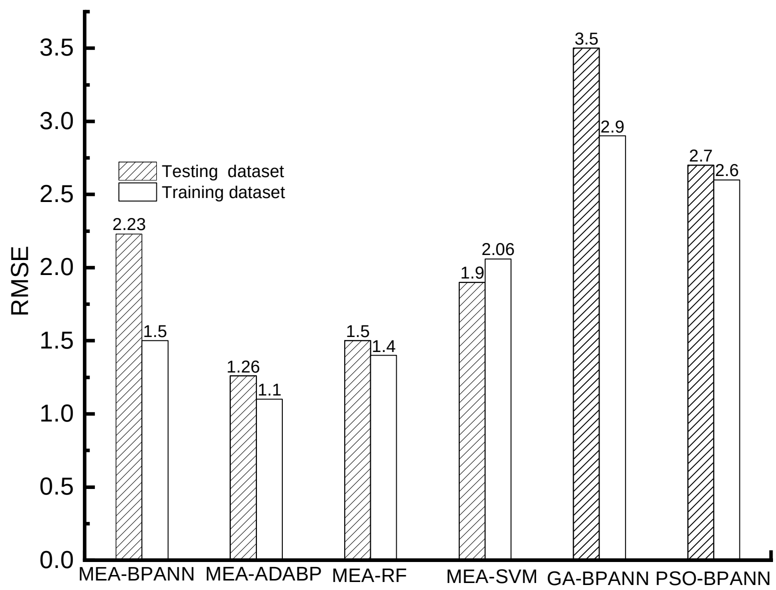

Figure.6 The RMSE of the models

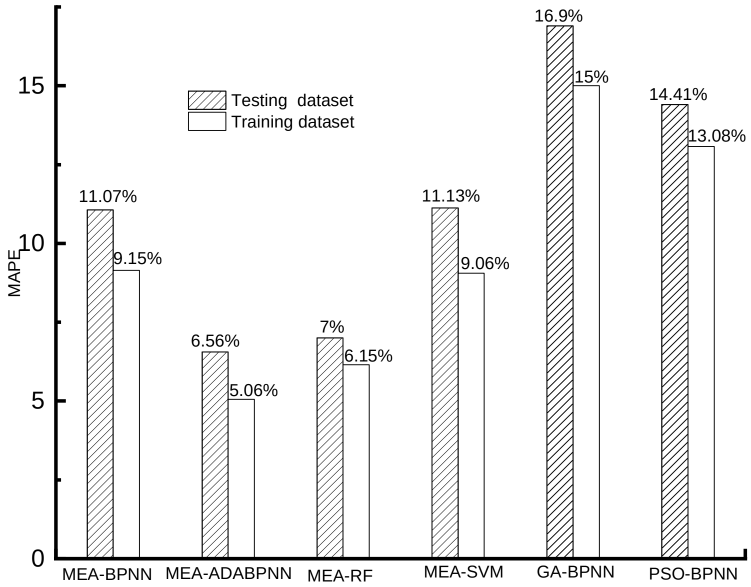

Figure.7 The MAPE of the models

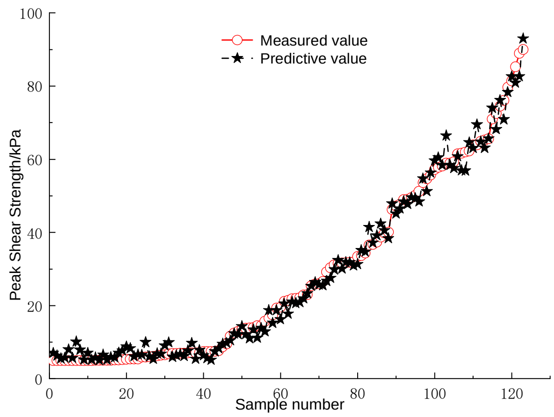

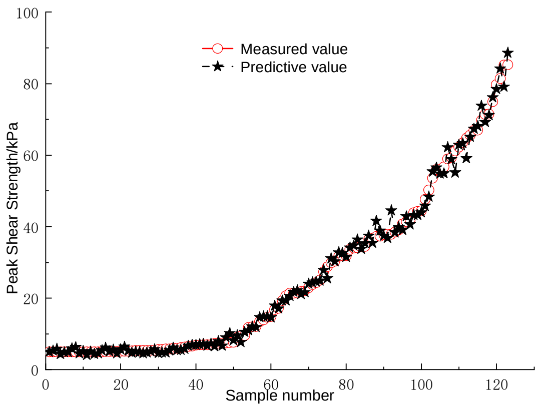

(a)MEA-BPANN (b)MEA-ADABPANN

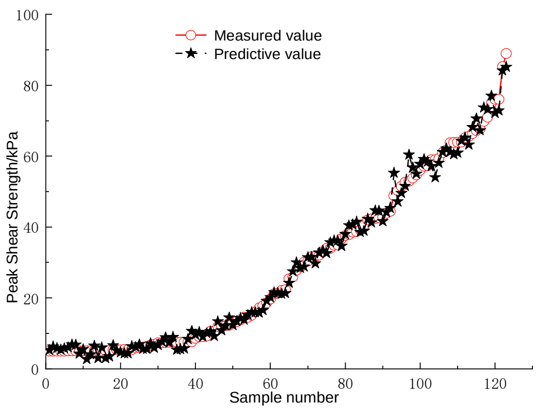

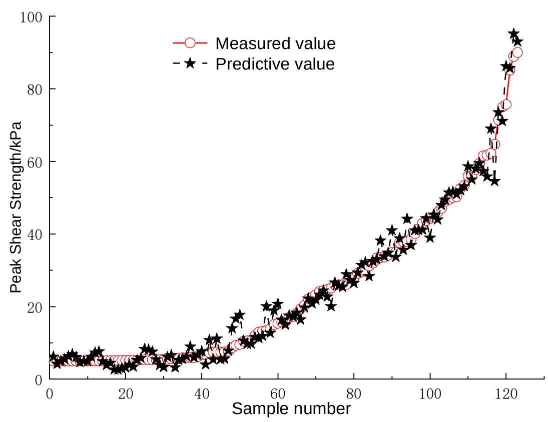

(c) MEA-RF (d) MEA-SVM

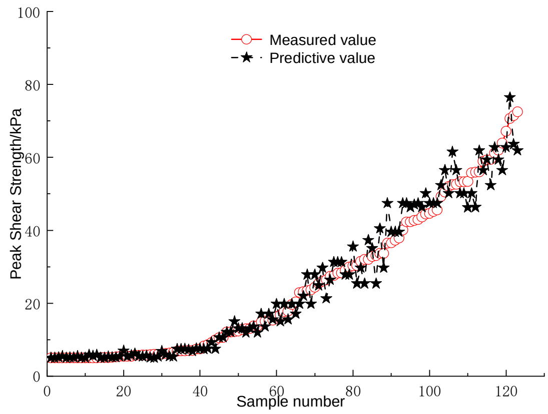

(e)GA-BPANN

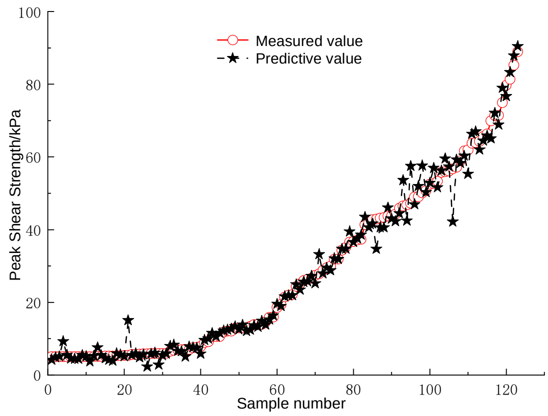

(f) PSO-BPANN

Figure.8 Predictive performance of the models for testing dataset

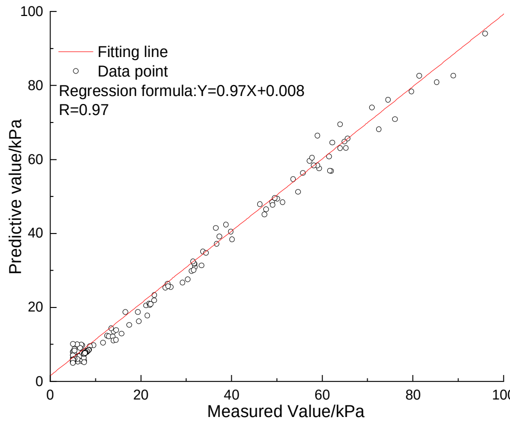

(a) MEA-BPANN

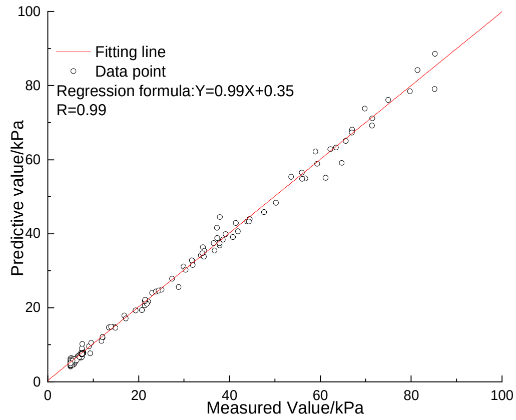

(b) MEA-ADABPANN

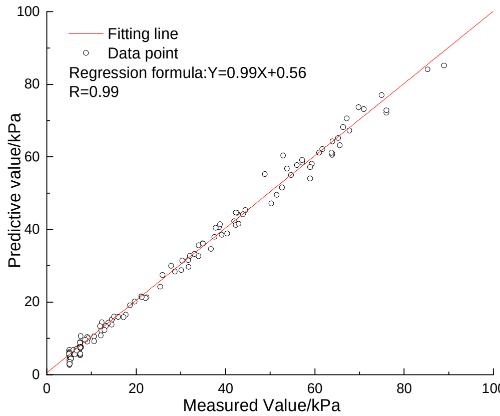

(c) MEA-RF

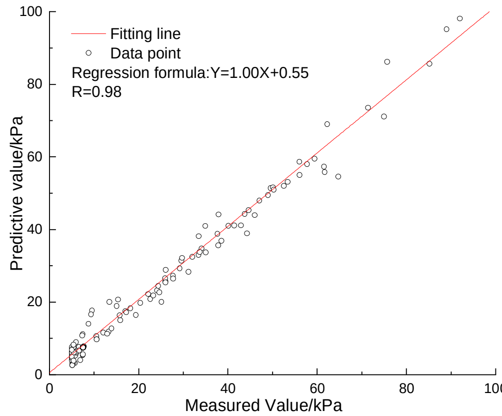

(d) MEA-SVM

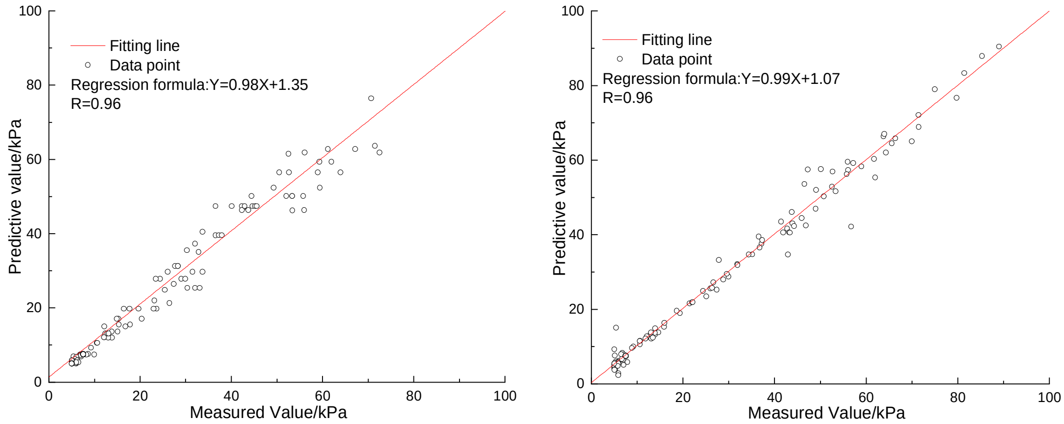

(e) GA-BPANN (f) PSO-BPANN

Figure.9 The R values of the established models for testing dataset

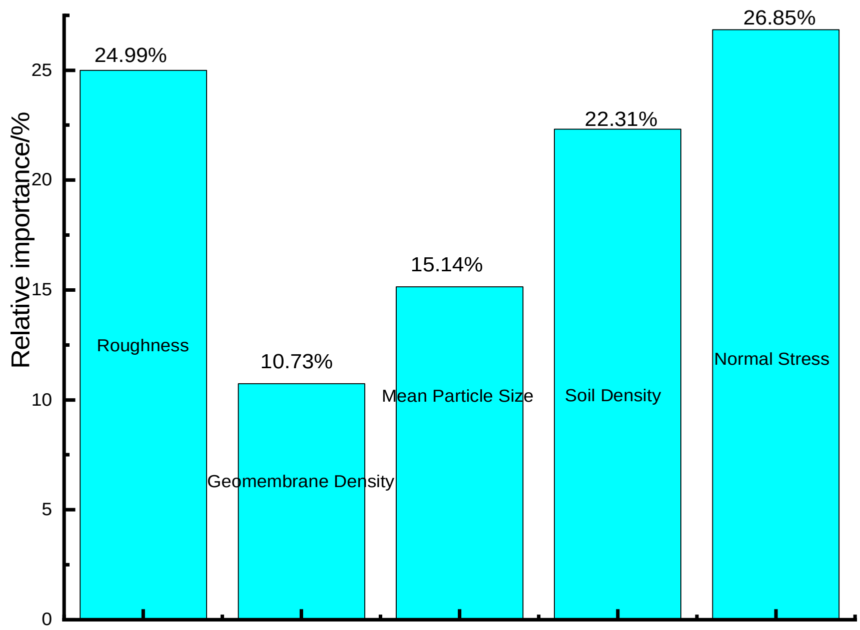

Figure.10 The relative importance of the input parameters for the model

Figure 11 The bespoke large direct shear apparatus

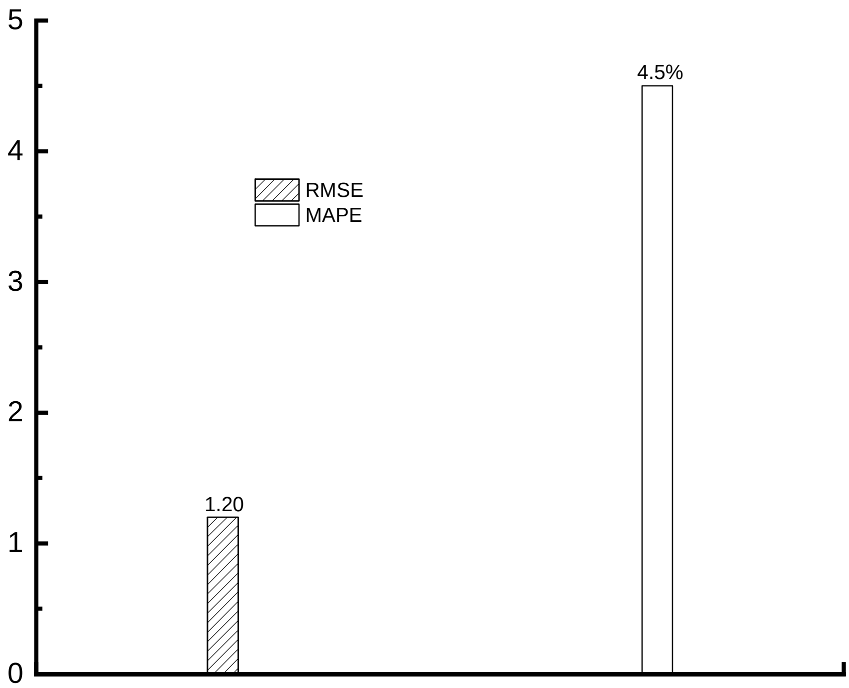

(a) The MAPE and RMSE

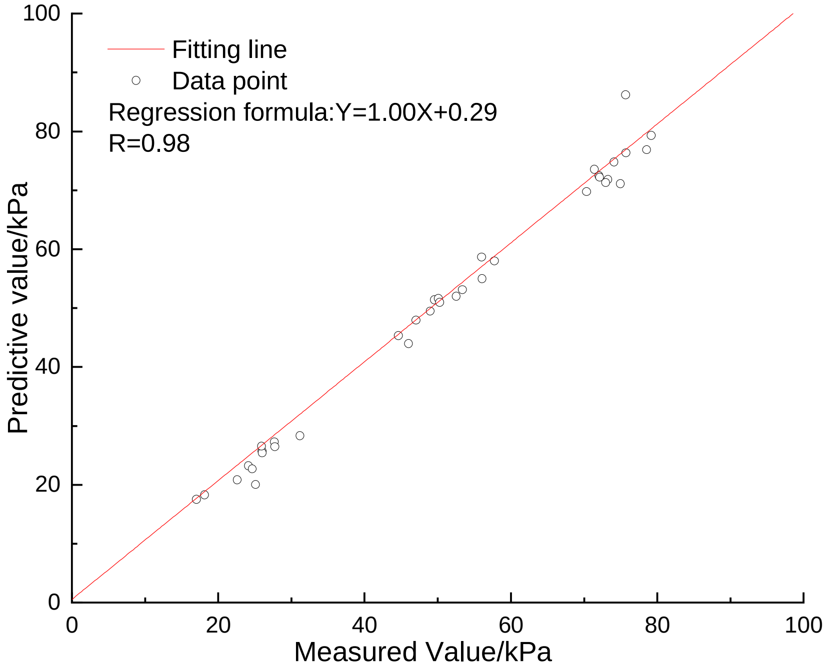

(b) The R values

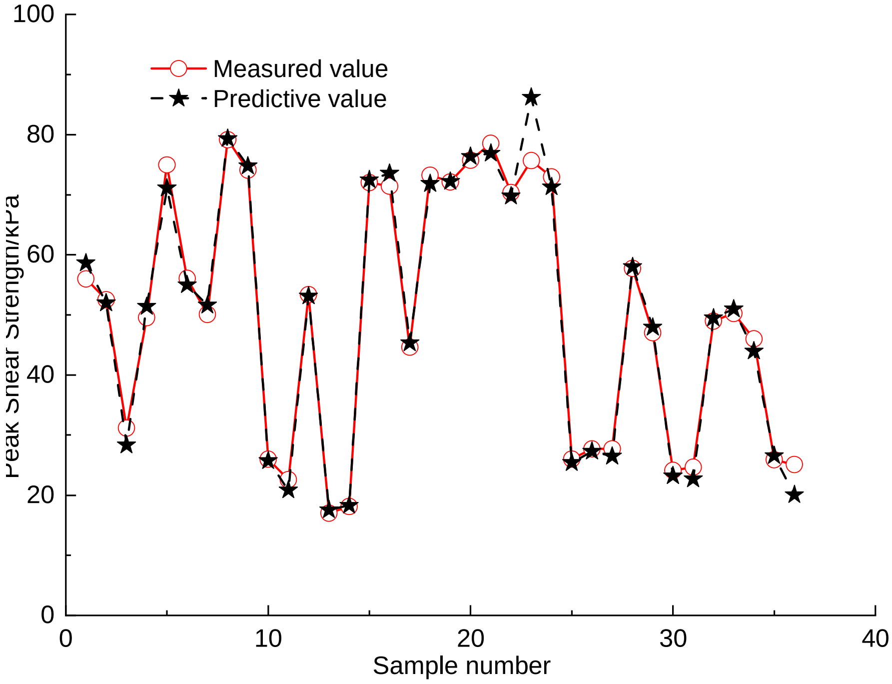

(c) The measured value and predictive value

Figure.12 The comparison between the predictive value and measured value

Appendix

Table 1 The measured and forecasting (MEA tuned ADABPANN model) peak shear strength based on training dataset

Sample number	Measured value/kPa	Predictive value/kPa	Sample number	Measured value/kPa	Predictive value/kPa
1	4.98963	5.07802	248	17.80523	17.72443
2	5.0045	5.0492	249	18.12017	18.40374
3	5.0045	4.84397	250	19.51123	18.90518
4	5.00467	4.93271	251	19.5468	19.27911
5	5.00467	4.95652	252	19.66293	20.25903
6	5.00467	5.09454	253	19.72097	19.46617
7	5.00467	5.2539	254	20.34617	19.99806
8	5.00507	5.00692	255	20.7342	20.70795
9	5.00507	5.09665	256	21.12613	20.88166
10	5.00533	4.91534	257	21.28817	21.33389
11	5.00533	4.89768	258	21.37983	21.40164
12	5.007	4.8383	259	21.37983	21.5139
13	5.00923	4.97298	260	21.4101	21.17619
14	5.0103	5.00663	261	21.81087	21.42961
15	5.0106	5.05668	262	21.81887	22.01384
16	5.01093	5.03141	263	21.8735	21.98134

17	5.01107	5.32606	264	21.92697	22.0788
18	5.01107	4.89651	265	22.07677	22.03291
19	5.01107	4.71498	266	22.34013	22.33551
20	5.01107	5.03137	267	22.50703	22.23603
21	5.01107	5.03295	268	22.58887	22.68524
22	5.01157	5.02131	269	22.9223	22.38097
23	5.01163	4.97625	270	22.9429	23.14558
24	5.01163	4.9925	271	22.94877	22.87615
25	5.01197	4.80726	272	23.09927	23.93126
26	5.01197	5.24233	273	23.12083	22.80502
27	5.01197	4.93095	274	23.2603	23.49023
28	5.01197	4.88095	275	23.4073	23.48387
29	5.01387	5.05977	276	23.43353	23.48377
30	5.0144	5.09428	277	23.6395	23.73335
31	5.01543	4.74563	278	23.65047	23.34193
32	5.0174	5.32093	279	23.80277	24.23564
33	5.0174	4.92562	280	24.11237	23.89553
34	5.0174	4.95219	281	24.456	24.52083
35	5.0174	5.16903	282	24.64353	24.07854
36	5.0174	5.08576	283	24.81677	24.45243

37	5.0174	4.81351	284	25.03057	25.12287
38	5.01837	5.04202	285	25.15917	25.45124
39	5.0189	5.114	286	25.4101	25.18061
40	5.02053	5.03654	287	25.91103	26.14373
41	5.02067	5.06551	288	25.9897	25.89893
42	5.02067	5.20021	289	26.01123	26.28924
43	5.0208	4.98198	290	26.05283	26.10484
44	5.0218	5.07275	291	26.30017	26.51344
45	5.0218	5.06584	292	26.42603	25.54996
46	5.02237	5.32235	293	26.51257	26.73967
47	5.02237	5.02325	294	26.58823	26.09942
48	5.031	4.8872	295	26.62177	26.19805
49	5.0334	5.03977	296	26.69823	26.50799
50	5.04093	5.06984	297	27.3689	27.23663
51	5.0434	5.01287	298	27.37453	27.40524
52	5.05707	4.92696	299	27.63683	27.32531
53	5.0794	5.19343	300	27.67417	27.39376
54	5.08113	5.26429	301	27.70037	27.68739
55	5.0851	5.14057	302	27.73193	27.97006
56	5.1032	5.01462	303	28.26457	28.05176

57	5.1032	5.08458	304	28.2884	28.68302
58	5.10437	5.25259	305	28.65633	28.09557
59	5.10783	5.21874	306	28.6728	28.40381
60	5.10783	5.1247	307	29.00937	29.77309
61	5.1114	5.30736	308	29.00973	28.96724
62	5.11427	4.88713	309	29.17603	28.31221
63	5.1179	5.0337	310	29.68633	29.68087
64	5.12013	5.1014	311	29.7254	29.39671
65	5.12527	5.06046	312	29.87927	29.80073
66	5.13073	4.88604	313	29.90637	30.37584
67	5.1326	5.27099	314	30.09703	30.27619
68	5.133	5.11708	315	30.12733	30.1202
69	5.14487	5.06434	316	30.26353	30.64537
70	5.16443	5.24242	317	30.3338	30.16687
71	5.16443	5.17223	318	30.33817	30.21384
72	5.1645	5.04707	319	30.69857	31.69109
73	5.17767	5.19027	320	30.77997	30.32424
74	5.2037	5.27955	321	31.11687	31.08049
75	5.2037	5.21016	322	31.16663	30.42662
76	5.245	5.00929	323	31.32127	31.06946

77	5.32653	5.24908	324	31.4833	31.71479
78	5.3427	5.6351	325	31.63737	31.72278
79	5.3607	5.47333	326	31.70173	31.69352
80	5.36353	5.31869	327	31.74587	31.76302
81	5.36397	5.62912	328	32.0227	32.35325
82	5.38203	5.11909	329	32.02433	32.35315
83	5.38983	5.28917	330	32.0281	32.14293
84	5.38983	5.23898	331	32.61193	32.53223
85	5.38983	5.20127	332	32.66667	32.8655
86	5.3914	5.57458	333	32.82073	32.67271
87	5.3952	5.37235	334	32.88243	33.40878
88	5.40263	5.31916	335	33.05787	33.66386
89	5.40527	5.2945	336	33.38763	33.14109
90	5.40917	5.358	337	33.46067	33.75001
91	5.41573	5.61987	338	33.67243	33.5604
92	5.41953	5.69533	339	33.6806	33.89067
93	5.4204	5.28449	340	33.9719	33.65009
94	5.4284	5.71246	341	33.97283	34.24466
95	5.4285	5.45992	342	34.04763	34.29186
96	5.43237	5.25915	343	34.08897	33.94024

97	5.44397	5.56081	344	34.16153	33.7672
98	5.4616	5.61706	345	34.46377	35.4418
99	5.4616	5.27269	346	34.8914	35.14616
100	5.47103	5.5425	347	34.9307	34.96779
101	5.47467	5.46305	348	35.01303	34.91844
102	5.54667	5.57498	349	35.59813	35.77878
103	5.57727	5.62197	350	35.62567	35.84006
104	5.61597	5.21574	351	35.8008	35.95788
105	5.62253	5.65073	352	35.9204	35.83796
106	5.6227	5.6862	353	35.95323	35.75037
107	5.65307	5.64172	354	36.17027	36.41214
108	5.65823	5.70763	355	36.51683	36.4906
109	5.68353	5.37265	356	36.71787	36.51876
110	5.71723	5.76076	357	37.01953	36.20828
111	5.7456	5.65065	358	37.02227	36.96472
112	5.7534	5.97745	359	37.09927	36.63357
113	5.75937	5.59294	360	37.25693	37.08615
114	5.79587	5.99137	361	37.54457	37.74418
115	5.8029	6.08486	362	37.63053	37.37945
116	5.91387	5.86617	363	37.82507	39.14103

117	5.9301	5.83733	364	37.86237	36.91003
118	5.95393	5.97267	365	37.8914	37.85298
119	5.95393	5.40554	366	38.54187	38.20868
120	5.97283	5.92433	367	38.5764	38.69053
121	6.005	6.35331	368	38.76217	38.82801
122	6.0119	6.1584	369	39.1442	39.10988
123	6.0487	5.78564	370	39.25557	40.75041
124	6.0515	6.08281	371	39.82833	39.80208
125	6.08903	6.01	372	40.088	40.08694
126	6.1367	6.61967	373	40.3617	40.50813
127	6.1367	5.66329	374	40.3633	40.26878
128	6.1675	6.27352	375	40.7665	41.37611
129	6.16947	6.17734	376	41.2302	41.37385
130	6.2388	6.18426	377	41.3971	41.74049
131	6.2406	6.39717	378	41.97417	42.093
132	6.2515	6.3385	379	42.2347	42.32597
133	6.26933	6.25964	380	42.30193	42.05932
134	6.3399	6.60174	381	42.3124	42.83674
135	6.4425	6.07212	382	42.58743	42.91668
136	6.4655	6.40768	383	42.91947	42.95701

137	6.48837	7.18974	384	43.2354	41.8651
138	6.56273	6.8693	385	43.70713	43.21928
139	6.63153	6.43624	386	43.78763	43.83929
140	6.6776	6.90931	387	44.43353	44.37035
141	6.7743	6.5724	388	44.6174	44.62862
142	6.79263	6.99635	389	45.1007	45.75384
143	6.81837	6.57984	390	45.16647	45.2411
144	6.8223	6.88225	391	45.567	45.73883
145	6.8323	6.82422	392	45.99813	45.65391
146	6.86577	7.0084	393	46.2425	46.34851
147	6.89587	7.14564	394	46.31343	46.38831
148	6.92013	6.91942	395	46.69023	46.52116
149	6.9204	7.00884	396	46.79063	46.69371
150	6.9253	6.67673	397	47.0226	46.82201
151	6.9253	6.85014	398	47.62307	47.07797
152	6.967	7.12431	399	48.72677	48.7121
153	7.00057	7.02298	400	48.8169	48.78101
154	7.04113	7.03075	401	49.28463	49.38233
155	7.04547	6.7516	402	49.53247	49.89743
156	7.06477	6.84282	403	49.9227	49.9743

157	7.14593	6.97156	404	50.0571	50.07712
158	7.2425	7.06854	405	50.2472	50.22192
159	7.2928	7.04531	406	50.49793	50.40154
160	7.32323	7.30035	407	50.49793	50.46894
161	7.3296	7.46737	408	51.26487	52.23906
162	7.35937	7.41881	409	51.41367	51.55574
163	7.41017	6.8707	410	51.4827	51.11751
164	7.4201	7.5335	411	51.9779	52.35609
165	7.42397	7.25342	412	52.0298	51.99041
166	7.4452	7.5043	413	52.0298	52.09067
167	7.46237	7.57266	414	52.06563	51.97341
168	7.47463	7.3393	415	52.63147	52.86024
169	7.47463	7.52335	416	52.63147	52.66028
170	7.48933	7.31126	417	52.92577	53.07435
171	7.48933	7.55272	418	53.3268	53.10408
172	7.50897	7.56226	419	53.37797	52.92729
173	7.51123	6.98844	420	53.3998	53.47349
174	7.5455	7.3651	421	53.4136	53.53974
175	7.58373	7.85638	422	53.59363	53.76704
176	7.62837	7.63078	423	53.7397	53.70204

177	7.6311	7.83514	424	53.76377	53.66007
178	7.69433	7.71038	425	54.6648	54.40681
179	8.0234	8.00109	426	54.67433	55.03933
180	8.2266	8.40791	427	55.75047	56.04385
181	8.5996	8.53534	428	55.95453	55.96601
182	8.74543	8.75723	429	56.00373	56.08052
183	9.03563	9.63425	430	56.4176	56.35413
184	9.06817	9.0528	431	57.06563	57.05669
185	9.2209	9.68442	432	57.20887	57.99208
186	9.31187	9.5828	433	57.2591	57.36418
187	9.3586	9.11948	434	57.716	57.59712
188	9.54703	9.73771	435	57.74533	57.69828
189	9.92877	9.94077	436	58.14607	57.53362
190	10.3117	9.63577	437	58.94803	58.64316
191	10.5033	10.55595	438	59.31757	59.32445
192	10.58423	10.79138	439	59.3998	58.16892
193	10.59403	10.8676	440	59.42883	59.39274
194	10.60383	10.54618	441	60.09643	60.17598
195	10.60877	10.66475	442	60.8483	60.99863
196	11.37983	10.95636	443	60.92223	60.22003

197	11.63577	11.6561	444	60.96723	61.3774
198	11.92323	12.432	445	61.17263	59.71476
199	12.02867	11.8618	446	61.5125	61.09872
200	12.05563	12.21936	447	61.5125	61.90787
201	12.08507	12.18683	448	61.66383	62.24597
202	12.09243	12.11599	449	62.23907	62.26768
203	12.10713	12.10037	450	63.3128	63.35639
204	12.11207	11.84367	451	63.45197	63.87651
205	12.147	12.63159	452	63.86987	63.34053
206	12.3012	12.67595	453	63.94803	63.75331
207	12.32397	12.15499	454	63.94803	64.19416
208	12.34013	12.42336	455	64.73047	63.99272
209	12.34013	12.27191	456	64.89647	64.74089
210	12.3532	12.1027	457	64.9074	64.94939
211	12.52133	12.37929	458	65.21837	65.06786
212	12.83763	12.63931	459	65.5955	65.92826
213	13.25467	13.02222	460	66.33277	66.29877
214	13.34643	13.11184	461	66.34213	66.04879
215	13.44313	13.27385	462	66.94663	67.33235
216	13.80277	13.56122	463	67.00953	66.61835

217	13.80277	13.74861	464	67.13693	68.13141
218	13.80967	14.13999	465	67.73033	68.34478
219	14.00307	13.86526	466	68.50547	68.94726
220	14.48877	14.89029	467	68.50547	68.49647
221	14.5206	14.37714	468	68.74627	68.77332
222	14.54843	14.63085	469	69.79853	70.11479
223	14.88013	14.59482	470	70.662	70.28036
224	14.9621	14.82797	471	70.97567	70.84823
225	14.96603	15.43531	472	71.48847	72.44146
226	15.01873	15.05842	473	71.48847	70.96544
227	15.06937	14.95706	474	72.48727	72.18602
228	15.07357	15.48237	475	73.6517	73.33734
229	15.13017	14.94777	476	74.52247	74.82406
230	15.15193	15.11312	477	74.9563	74.88234
231	15.24337	15.5998	478	75.6814	76.07491
232	15.338	15.33021	479	76.0589	74.79237
233	15.3668	15.54132	480	76.0589	76.13051
234	15.72567	15.94605	481	78.2088	78.53151
235	15.73383	15.93981	482	78.6147	79.03132
236	15.90337	15.82833	483	79.68913	79.59337

237	16.02997	16.54653	484	79.73807	79.7459
238	16.41387	16.01572	485	81.4	81.55158
239	16.58283	16.50846	486	83.0852	83.33479
240	16.77137	16.5493	487	83.2013	82.71408
241	16.7923	16.73105	488	83.7864	83.77879
242	16.8657	17.26988	489	85.17213	84.51494
243	17.02153	17.44643	490	85.26403	85.05255
244	17.18637	17.01505	491	88.9224	89.27866
245	17.22473	17.40464	492	90	91.72707
246	17.43633	17.3824	493	90	93
247	17.6854	17.46771			

Table 2 The measured and forecasting (MEA tuned ADABPANN model) peak shear strength based on testing dataset

Sample number	Measured value/kPa	Predictive value/kPa	Sample number	Measured value/kPa	Predictive value/kPa
1	5.0045	5.01671	63	17.80523	15.54409
2	5.00467	5.01312	64	19.66293	19.79633
3	5.00467	5.17053	65	20.34617	17.08303
4	5.00533	5.47349	66	22.9429	19.79633
5	5.01093	5.01671	67	23.12083	22.00805

6	5.01107	5.14725	68	23.43353	27.85485
7	5.01107	5.15521	69	23.6395	19.79633
8	5.01157	5.47349	70	24.37733	27.85485
9	5.01197	5.08162	71	25.4101	24.87685
10	5.01197	5.01312	72	26.05283	29.71089
11	5.01387	5.87492	73	26.42603	21.31825
12	5.0174	5.5447	74	27.3689	26.44658
13	5.0218	5.87492	75	27.63683	31.28891
14	5.08603	5.0667	76	28.26457	31.28891
15	5.1032	5.0667	77	28.2884	31.28891
16	5.10783	5.38427	78	29.00973	27.85485
17	5.14487	5.16805	79	29.90637	27.85485
18	5.245	5.16805	80	30.26353	35.56025
19	5.40263	5.41844	81	30.33817	25.38823
20	5.40527	6.96774	82	31.4833	29.71089
21	5.41953	5.41844	83	32.0227	25.38823
22	5.47103	5.72903	84	32.02433	37.29152
23	5.7456	6.2094	85	32.82073	35.07781
24	5.7534	5.47349	86	33.05787	25.38823
25	5.8029	5.38427	87	33.67243	40.50028

26	5.82017	5.61752	88	33.6806	29.71089
27	5.91387	5.08162	89	36.51683	47.42909
28	5.95393	5.0667	90	36.52903	39.57714
29	6.005	5.38427	91	37.25693	39.59725
30	6.0515	6.86249	92	37.8914	39.59725
31	6.2406	5.87492	93	40.088	47.42909
32	6.3399	5.41844	94	42.30193	47.42909
33	6.48837	5.38427	95	42.3124	46.34628
34	6.8223	7.4201	96	42.72283	47.08162
35	6.9253	7.4201	97	42.91947	47.42909
36	6.92753	7.47898	98	43.70713	46.34628
37	7.0304	7.24752	99	44.43353	50.15926
38	7.04547	6.86249	100	44.6174	47.42909
39	7.42397	7.58427	101	45.16647	47.42909
40	7.48933	7.58427	102	45.567	47.42909
41	8.2266	7.4201	103	49.28463	52.38813
42	8.5996	7.58427	104	50.49793	56.50637
43	9.2209	9.2818	105	52.0298	50.15926
44	9.92877	7.47898	106	52.52247	61.54773
45	10.5033	10.60262	107	52.63147	56.50637

46	10.59403	10.60262	108	53.3268	50.15926
47	12.09243	12.0818	109	53.3268	50.15926
48	12.11207	12.0818	110	53.37797	46.26868
49	12.147	15.0002	111	55.75047	50.15926
50	12.3532	13.1151	112	55.95453	46.34628
51	12.83763	13.1151	113	56.0618	61.89379
52	13.01737	11.96599	114	58.94803	56.50637
53	13.09263	13.1151	115	59.31757	59.38752
54	13.80277	13.63866	116	59.3998	52.38813
55	13.80967	11.96599	117	61.17263	62.78907
56	14.88013	17.08303	118	61.95413	59.38752
57	15.07357	13.63866	119	63.94803	56.50637
58	15.24337	17.08303	120	67.13693	62.78907
59	15.338	15.54409	121	70.662	76.4683
60	16.41387	19.79633	122	71.48847	63.62928
61	16.77137	15.0002	123	72.48727	61.89379
62	17.6854	19.79633			